



**Evaluation and Wind Tunnel Tests
of the 4,000-lb (Normal-Force)
Pitch/Yaw and Roll-Damping Stability
Balance Systems for Measuring Direct,
Cross, and Cross-Coupling Derivatives**

**T. D. Buchanan, S. M. Coulter, and E. J. Marquart
ARO, Inc.**

September 1981

Final Report for Period June 5, 1978 — May 25, 1979

Approved for public release; distribution unlimited.

**ARNOLD ENGINEERING DEVELOPMENT CENTER
ARNOLD AIR FORCE STATION, TENNESSEE
AIR FORCE SYSTEMS COMMAND
UNITED STATES AIR FORCE**

NOTICES

When U. S. Government drawings, specifications, or other data are used for any purpose other than a definitely related Government procurement operation, the Government thereby incurs no responsibility nor any obligation whatsoever, and the fact that the Government may have formulated, furnished, or in any way supplied the said drawings, specifications, or other data, is not to be regarded by implication or otherwise, or in any manner licensing the holder or any other person or corporation, or conveying any rights or permission to manufacture, use, or sell any patented invention that may in any way be related thereto.

Qualified users may obtain copies of this report from the Defense Technical Information Center.

References to named commercial products in this report are not to be considered in any sense as an indorsement of the product by the United States Air Force or the Government.

This report has been reviewed by the Office of Public Affairs (PA) and is releasable to the National Technical Information Service (NTIS). At NTIS, it will be available to the general public, including foreign nations.

APPROVAL STATEMENT

This report has been reviewed and approved.



ELTON R. THOMPSON
Director, Project Analysis
and Engineering
Deputy for Operations

Approved for publication:

FOR THE COMMANDER



JOHN M. RAMPY
Director of Aerospace Flight Dynamics Test
Deputy for Operations

UNCLASSIFIED

REPORT DOCUMENTATION PAGE		READ INSTRUCTIONS BEFORE COMPLETING FORM
1 REPORT NUMBER AEDC-TR-80-12	2 GOVT ACCESSION NO.	3 RECIPIENT'S CATALOG NUMBER
4 TITLE (and Subtitle) EVALUATION AND WIND TUNNEL TESTS OF THE 4,000-LB (NORMAL-FORCE) PITCH/YAW AND ROLL DYNAMIC STABILITY BALANCE SYSTEMS FOR		5 TYPE OF REPORT & PERIOD COVERED Final Report - June 5-8, 1978 - May 18-25, 1979
		6 PERFORMING ORG REPORT NUMBER
7 AUTHOR(s) T. D. Buchanan, S. M. Coulter, and E. J. Marquart, ARO, Inc., a Sverdrup Corporation Company		8 CONTRACT OR GRANT NUMBER(s)
9 PERFORMING ORGANIZATION NAME AND ADDRESS Arnold Engineering Development Center/DO Air Force Systems Command Arnold Air Force Station, TN 37389		10. PROGRAM ELEMENT, PROJECT, TASK AREA & WORK UNIT NUMBERS Program Element 65807F
11 CONTROLLING OFFICE NAME AND ADDRESS Arnold Engineering Development Center/DOS Air Force Systems Command Arnold Air Force Station, TN 37389		12. REPORT DATE September 1981
		13 NUMBER OF PAGES 75
14 MONITORING AGENCY NAME & ADDRESS (if different from Controlling Office)		15. SECURITY CLASS. (of this report) UNCLASSIFIED
		15a DECLASSIFICATION/DOWNGRADING SCHEDULE N/A
16 DISTRIBUTION STATEMENT (of this Report) Approved for public release; distribution unlimited.		
17 DISTRIBUTION STATEMENT (of the abstract entered in Block 20, if different from Report)		
18 SUPPLEMENTARY NOTES Available in Defense Technical Information Center (DTIC).		
19 KEY WORDS (Continue on reverse side if necessary and identify by block number) dynamic tests damping (pitch, yaw, roll) external stores wind tunnel tests forced oscillation aerodynamic stability cross derivatives dynamic response cross-coupling derivatives high angle of attack F-16 aircraft		
20 ABSTRACT (Continue on reverse side if necessary and identify by block number) Early in the 1970's, the personnel at the Arnold Engineering Development Center (AEDC) recognized the need for a set of new dynamic test mechanisms for testing aircraft models at high angles of attack. At these angles of attack cross and cross-coupling derivatives may be significant in determining the aircraft's stability. Dynamic balances were fabricated to perform pitch, yaw, and roll dynamic stability tests of aircraft or large missile		

UNCLASSIFIED

UNCLASSIFIED

4. TITLE (Continued)

MEASURING DIRECT, CROSS, AND CROSS-COUPLING DERIVATIVES

20. ABSTRACT (Continued)

models at AEDC. The balances were designed to measure not only the direct derivatives but also cross and cross-coupling derivatives. The set of balances comprises a 4,000-lb (normal-force) roll and a 4,000-lb pitch/yaw forced-oscillation balance to measure the direct damping derivatives and a five-component can-type balance to measure the cross and cross-coupling derivatives attributable to pitch or yaw. Extensive laboratory investigations of the balances' static and dynamic response characteristics were performed before wind tunnel tests of a 1/9-scale F-16A model in the AEDC Propulsion Wind Tunnel (16T) at Mach numbers from 0.2 to 1.4. Laboratory-simulated loads indicated the rolling-moment load cells of the can balance had a low natural frequency which could cause significant magnification and phase shift errors to occur in the cross-coupling derivative results of the tests. The study has shown that the 4,000-lb pitch/yaw balance is operational for measuring direct derivatives at angles of attack up to 50 deg, and the roll balance is operational for measuring direct derivatives at angles of attack up to 15 deg.

PREFACE

The work reported herein was conducted by the Arnold Engineering Development Center (AEDC), Air Force Systems Command (AFSC), as an in-house development project at the request of the Director of Analysis and Evaluation (DOA), Arnold Air Force Station, Tennessee. The model was funded by the Air Force Armament Test Laboratory (AFATL/DLJC). J. M. Rampy, DOA, was the Air Force project manager. The results of the tests will be used to support the AEDC Dynamic Stability Analysis Project P43C-03. R. W. Butler and G. H. Saunders, Jr., of ARO, Inc., were the Dynamic Stability Analysis project monitors. The results were obtained by ARO, Inc., AEDC Group (a Sverdrup Corporation Company), operating contractor for the AEDC, AFSC, Arnold Air Force Station, Tennessee. Tests were conducted in the Propulsion Wind Tunnel (16T) of the AEDC Propulsion Wind Tunnel Facility, under ARO Project Numbers P41T-00, P41T-DOE, and P41T-02 in two phases: roll-damping (June 5 through June 8, 1978), and pitch-and yaw-damping (May 18 through 25, 1979). This manuscript was submitted for publication on February 4, 1980.

AEDC-TSR-79-P50, written by T. D. Buchanan, S. M. Coulter, and E. J. Marquart in July 1979 documents the complete set of results obtained from the wind tunnel tests.

The authors wish to acknowledge the efforts of Messrs. W. E. Carelton, P. G. Lucas, R. R. Turney, R. W. Butler, and W. H. Comer during the development of these balances. The authors also acknowledge R. G. Butler, S. P. Northcutt, H. C. Hall, Jr., K. D. Carter, J. W. Wilson, G. R. Mattasits, R. D. Morris, Jr., and others who significantly contributed to the accomplishment of this task.

Messrs. Buchanan, Coulter, and Marquart are currently employed by Calspan Field Services, Inc., AEDC Division.

CONTENTS

	<u>Page</u>
1.0 INTRODUCTION	5
2.0 BALANCE SYSTEMS	5
3.0 LABORATORY EVALUATION	7
4.0 WIND TUNNEL TESTS	
4.1 Apparatus	
4.1.1 Test Facility	9
4.1.2 Test Article	10
4.2 Model Oscillation Control Checks	11
4.3 Test Description	
4.3.1 Test Conditions	12
4.3.2 Data Acquisition	13
4.3.3 Data Reduction	13
4.3.4 Uncertainty of Measurements	13
4.4 Results and Discussion	15
5.0 SUMMARY	16
6.0 RECOMMENDATIONS	17
REFERENCES	17

ILLUSTRATIONS

Figure

1. History of 4,000-lb Mechanism Development	19
2. 4,000-lb Pitch/Yaw Balance System	20
3. 4,000-lb Roll Balance System	23
4. Inertia Loading Evaluation	24
5. Frequency Effects on Balance Load-Measuring Elements	26
6. Installation of the Models in the Propulsion Wind Tunnel (16T) Test Section	27
7. F-16A Model Details	31
8. Photographs of Typical F-16A Configurations	36
9. Details of External Stores	39
10. Forced-Oscillation Balance Control and Readout System Block Diagram	44
11. Static Normal-Force Coefficient	45

<u>Figure</u>	<u>Page</u>
12. Longitudinal Stability Results	46
13. Lateral Stability Results	48
14. Effects of External Stores on the Damping Derivatives at $M = 0.8$	49
15. Effect of Mach Number on the Damping Derivatives	50
16. Static Yawing-Moment Derivative, $C_{n\dot{\beta}} \sin \alpha$	51
17. Cross and Cross-Coupling Derivative Results	52

TABLES

1. Balance Design Capabilities	54
2. Natural Frequency Effects	55
3. Aircraft Stores Details, Configuration 3	56
4. Aircraft Stores Details, Configuration 5	57
5. Aircraft Stores Details, Configuration 11	58
6. Configuration Chart	59
7. Typical Installation Natural Frequencies	60
8. Test Summary	61
9. Uncertainties	63

NOMENCLATURE	72
--------------------	----

1.0 INTRODUCTION

Researchers in flight characteristics of aircraft at high angles of attack have expressed the view that the lateral and longitudinal degrees of freedom may be coupled (Ref. 1). A recent conclusion by the Advisory Group for Aerospace Research and Development (AGARD) Fluid Dynamics Panel (Ref. 2) was that these coupling effects have been found to be very significant at high angles of attack. The panel also voiced concern about all the dynamic stability parameters of an aircraft operating at high angles of attack. Recommendations of the panel included obtaining a complete set of aerodynamic data to determine the importance of cross-coupling for the same test conditions in the same wind tunnel with the same support geometry.

Although the need for a dynamic stability test system to accomplish this task was anticipated by AEDC early in the 1970's, the development of systems based on new concepts generally requires several years, as exemplified by Fig. 1. A set of balances was designed to obtain the static and dynamic data, including cross and cross-coupling derivatives. The set comprises 4,000-lb (normal-force) and 1,500-lb pitch or yaw (P/Y) and roll forced-oscillation balance systems. This report describes the 4,000-lb balance systems. The response characteristics of the balances to static and dynamic loads were investigated in the laboratory, and wind tunnel tests with a 1/9-scale F-16A model were conducted in the AEDC Propulsion Wind Tunnel (16T).

The objectives of the wind tunnel tests were to obtain pitch, yaw, and roll-damping coefficients by means of the forced-oscillation technique on the F-16A model with external stores, and to investigate the requirements for measuring dynamic cross and cross-coupling derivative moments on an aircraft at high angles of attack. Data were obtained at Mach numbers from 0.2 to 1.4 at Reynolds numbers per foot of 1.2×10^6 and 2.4×10^6 . The angle-of-attack range was -5 to 45 deg for the roll test and -3 to 50 deg for the pitch and yaw tests. The reduced frequency ranged from 0.014 to 0.120 for the pitch-damping, 0.054 to 0.319 for the yaw-damping, and 0.040 to 0.360 for the roll-damping tests. Representative results will be presented. This report will emphasize the balance performance rather than analyze the aircraft flight characteristics.

2.0 BALANCE SYSTEMS

The objective of the designs was to build a set of basic forced-oscillation balances with added capability to determine cross and cross-coupling derivatives. A list of the desired derivative capabilities is shown in Table 1. The direct derivatives in pitch, yaw, and roll would be primarily reduced from the basic balance (P/Y or roll balance) signals. The basic balance would also provide the model oscillation. The cross and cross-coupling derivative

measurements would be obtained from optional balances. A P/Y balance is shown in Fig. 2a, and its external five-component can balance is shown in Fig. 2b. A schematic of this arrangement is shown in Fig. 2c. For the roll case, the cross-derivative balance could be designed as an integral part of the balance system as shown in Fig. 3. The balances are sized for aircraft models typical of the AEDC Tunnels 16T and 16S.

The P/Y and roll balances use the same principle of operation and control. Each balance consists of a cross-flexure pivot connected to a hydraulic cylinder through a force-measuring flexure. The hydraulic cylinder is operated with a servo valve to obtain sinusoidal oscillation motion at a constant oscillation amplitude, up to ± 2 deg, and constant frequency from 2 to about 10 Hz. The cross flexure is instrumented to measure angular displacement, to support the model loads (up to 4,000-lb normal force and 1,000-lb axial force), and to provide the restoring moment to cancel the inertia moment when the system is operating at the natural frequency of the model/balance assembly. The restoring moment of the P/Y balance can be changed by installing leaf springs on the sides of the balance; however, leaf springs were not used for these tests. The restoring moment was 6,295 ft-lb/rad for the P/Y balance and 1,468 ft-lb/rad for the roll balance. The P/Y balance was oriented at 0 deg with respect to the model for the pitch tests and at 90 deg for the yaw tests.

Systems for setting the oscillation frequency and oscillation amplitude and for nulling the static torque are provided by the balance control instrumentation. An electronic position feedback loop is used to maintain a constant oscillation amplitude and frequency under aerodynamic loads and permits testing both dynamically stable and unstable configurations. Data are normally obtained at the natural frequency of the model/flexure spring-mass system. Limit circuits are set before the test to provide overload protection for the balance. These limit circuits automatically shut the system down when their limits are exceeded. The torque-nulling system commands the hydraulic-driven piston in such a way that the force-measuring flexure (termed "torque beam") is not subjected to the model static aerodynamic moment. This allows the use of a torque beam suitable to the particular model. The 50.0-ft-lb-torque beam was used for this test on the P/Y balance, and a 16.7-ft-lb-torque beam was used for the roll balance.

Each load-measuring element of each balance is instrumented with three sets of strain gages. Two sets of these strain gages are used in this system for each dynamic measurement. A two-phase oscillator provides $E \sin \omega t$ (a-c) excitation to one set of strain gages to resolve the in-phase (with respect to a reference signal) component of the dynamic signal, whereas $E \cos \omega t$ (a-c) excitation is used to excite the second set of strain gages to resolve the out-of-phase (quadrature) component (where ω is the oscillation rate of the model). The third set of gages is d-c excited to provide readings of static deflections, forces, and moments. An LSI-11 minicomputer and filter-amplifier chassis are used to provide analog-to-digital

conversion and signal conditioning. The gage signals first pass through a 2-Hz passive filter, then through a 0.2-Hz active filter. A digital filter routine is performed in the minicomputer. The digital filter parameters can be changed easily, depending on the noise of the data. The 32 channels of data are then sent to the facility computer for on-line data reduction.

3.0 LABORATORY EVALUATION

The response characteristics of the balance load elements were investigated in two phases: a static calibration and a dynamic evaluation. The static calibrations were performed on each balance using standard calibration practices and methods. Those calibrations yielded the basic measuring element scale factors and interactions. Further discussion of those results will not be addressed. Inertia effects and a magnetic damper were used to apply known dynamic loads to the various balance load-measuring elements. Comparisons were made between the values from the data reduction equations and the known impressed loads.

The load elements of the balance experienced inertia (in-phase) loads when the balance system was oscillated. For example, the measured moments for the in-phase torque gage of the P/Y balance and the in-phase pitching moment from the can balance are shown in Fig. 4 for two oscillation frequencies representative of the frequencies expected during the wind tunnel tests. The agreement between the calculated values and the measured levels was within the uncertainty of calculated inertia load, based on the propagation of errors in M_{θ_f} , ω , and $\bar{\theta}$. This close agreement was also typical of the roll balance torque and can balance yawing-moment element response to inertia loads.

Selected elements of the balances were subjected to known damping moments by a magnetic damper. The level of damping was varied from 0 to 7 ft-lb-sec in small increments, at various oscillation frequencies ranging up to 9 Hz to determine the dynamic responses of the load-measuring elements. The output of each balance gage was fitted by a least-squares straight line as a function of damping moment for each frequency. The results show (Fig. 5) that for frequencies of practical interest, the P/Y and roll balances and the pitching-moment element of the can balance accurately measure the damping (Fig. 5a).

A corresponding check of the rolling-moment element of the can balance and yawing-moment element of the roll balance showed errors attributable to vibration effects. Simple one-degree-of-freedom theory (Ref. 3) gives

$$\text{Magnification} = \frac{\text{Balance Output}}{\text{Magnetic Damper}} = \left[1 - (f/f_n)^2 \right]^{-1}$$

$$\Delta\phi \approx \frac{2\delta f/f_n}{\left[1 - (f/f_n)^2\right]}$$

for $f/f_n \ll 1$ and δ small.

The magnification for the rolling-moment element of the can balance is shown in Fig. 5b. A curve fit of the theory to the data gives a natural frequency of 16.5 Hz. The phase shifts associated with these oscillation frequencies are shown in Fig. 5c. The value of damping (δ) that best matches the theory to these shifts is 0.040. Lower oscillation frequencies were not practical because of the inertia range obtainable with calibration equipment that was available. The response of the yawing-moment load element of the roll balance is shown in Fig. 5d. The natural frequency for the yawing-moment element was 40.8 Hz; therefore, the phase shift was very small, usually less than 1 deg. Higher oscillation frequencies were not practical because of the basic rolling-moment inertia of the system.

The simulated cross and cross-coupling loads indicated that vibration errors in these derivatives would be produced by magnification and phase shifting during wind tunnel tests. The magnitude of these errors depends on the level of aerodynamic damping and model moments of inertia. Based on the estimated mass moments of inertia of the F-16A model, the natural frequencies of the balance cross and cross-coupling elements are given in Table 2. The table shows estimated errors in the measured derivatives caused by magnification for an oscillation frequency of 6 Hz. The error attributable to magnification is a bias error in the data that could easily be compensated, but the phase shift is dependent on the aerodynamic damping. Correcting the cross or cross-coupling damping data from these low-frequency elements for both magnification and phase-shift errors is a task beyond the scope of this report, but the task must be addressed formally before cross and cross-coupling data from future tests can be quoted with known accuracy.

The laboratory evaluations verified that the direct derivatives are accurately resolved from the dynamic loads by the basic balances. The results indicated that the can balance should be capable of resolving the direct derivatives also.

4.0 WIND TUNNEL TESTS

Wind tunnel tests were conducted in Tunnel 16T at Mach numbers ranging from 0.2 to 1.4 using the 4,000-lb P/Y and roll balance systems. The model was a 1/9-scale F-16A configuration. These wind tunnel tests revealed problems in roll-oscillation control with the roll balance and unanticipated high dynamic loads on the P/Y balance.

During the roll test, the model roll oscillation could not be controlled at moderately high angles of attack except at low Mach numbers. Because of this problem the roll derivative test phase was normally limited to low angles of attack. The cause of the problem and its impact on the tests is discussed in detail in Section 4.2.

During the pitch/yaw tests, the interaction of the wind tunnel flow with the model excited the model in roll, and the rolling-moment elements of the can balance broke from fatigue. Analysis of the test data indicated the failure occurred early in the first high-angle-of-attack, pitch-oscillation phase. Further analysis of the data showed that the primary derivatives, i.e., $C_{m\alpha}$ and $C_{mq} + C_{m\dot{\alpha}}$, $C_{n\beta} \cos \alpha$, and $C_{nr} - C_{n\dot{\beta}} \cos \alpha$, from the P/Y balance, and static data, i.e., C_N , C_Y , C_n , and C_m , from the can balance were unaffected by the broken members, but the derivative data from the can balance were not reliable after the failure occurred. Only limited cross and cross-coupling results were obtained during the pitch-oscillation phase. Also, comparison between the P/Y balance and can balance (which also measures $C_{m\alpha}$ and $C_{mq} + C_{m\dot{\alpha}}$, for example) derivative data can only be made for test points preceding the load element failure. Direct derivatives from the P/Y balance and static data (from the can balance) were obtained for an angle-of-attack range from generally -3 to 50 deg for the clean wing configurations in pitch and yaw planes of oscillation. External store effects were investigated for low angles of attack (i.e., $\alpha < 25$ deg), and leading-edge flap and nose-strake effects were investigated at high angles of attack ($\alpha > 20$ deg). The results from the wind tunnel test are presented in this report to indicate the performance of the balances.

At present there are no analytical or empirical means available to estimate the level of the cross and cross-coupling data. Therefore, these data will be presented to illustrate their magnitudes, although the estimated uncertainty levels were usually larger than the measured levels except for $C_{n\beta} \sin \alpha$ from the roll balance, and $C_{lq} + C_{l\dot{\alpha}}$ and the static derivative $C_{l\alpha}$ from the can balance.

4.1 APPARATUS

4.1.1 Test Facility

Tunnel 16T is a variable-density, continuous-flow tunnel capable of being operated at Mach numbers from 0.2 to 1.6 and at stagnation pressures from 120 to 4,000 psfa. The maximum attainable Mach number can vary slightly depending upon the tunnel pressure ratio requirements with a particular test installation. The maximum stagnation pressure attainable is a function of Mach number and available electrical power. The tunnel stagnation temperature can be varied from about 80 to 160°F depending upon the available

cooling water temperature. The test section is 16 ft square by 40 ft long and is enclosed by 60-deg inclined-hole perforated walls of six-percent porosity. Additional information about the tunnel is presented in Ref. 4.

The general arrangements of the test section with the test articles installed are shown in Fig. 6. The balance-sting assembly is mounted in the auxiliary high-pitch mechanism which, in turn, is mounted in the 16T pitch sector for the pitch-yaw test (Fig. 6c) or the strut-mounted support for the roll test (Fig. 6d). These systems were used because it was possible to make modifications to stiffen the support mechanism, a necessity for dynamic testing. Hydraulic cylinders preload the main pivot bearing. Guy rods extend from the sector through the tunnel walls to hydraulic cylinders which serve to stiffen and preload the system in the pitch and yaw planes. Because of limited travel capability of the pitch drive motor for the pitch-yaw tests, the total angle-of-attack range had to be achieved by sweeping from -3 to 25 deg, resetting the support mechanism, and then sweeping from 20 to 50 deg. For yaw-damping tests, the P/Y balance is rolled 90 deg with respect to the model and main support system. The support pitch mechanism for the roll test could sweep through the complete angle of attack without resetting the support.

4.1.2 Test Article

The models used in the test were 1/9-scale versions of the F-16A of the dimensions shown in Fig. 7. Photographs of the configurations are presented in Fig. 8. The model assembly consisted of a centerbody section fabricated from steel onto which were bolted the aluminum wings, tail surfaces, and a fiberglass fuselage shell. The center-of-gravity of the assembly was adjusted to the moment reference point at fuselage station 35.628 by adjusting internal weights selected for each configuration of external stores. Two models were used, a pitch/yaw and a roll model, but both models used the same wings, tail surfaces, and external stores. The external stores are shown in Fig. 9. The pylons for the stores were attached to the wing by screws through the wings from the top surface. The boundary-layer-trip location is shown in Fig. 7e. A fairing (Fig. 6c) was used over the inlet at low angles of attack (-3 to 24 deg), but no fairing (Fig. 8a) was used for the high-angle-of-attack range (20 to 50 deg). The wings featured leading-edge flaps (Fig. 8a) set at either 0 or 25 deg by brackets bolted to the underside of the wings. There were no trailing-edge flaps on these wings. The horizontal tail surfaces were mounted on a pivot featuring a 72-tooth clutch-face mounting, thereby allowing these surfaces to be deflected in 5-deg increments. The vertical tail was rigid and had no deflectable rudder.

The models were fabricated at AEDC using existing F-16A model components for tracing wing contours, external stores, and fuselage body lines. Typical model weights and

mass moments of the inertia for the configurations are given in Tables 3, 4, and 5. A description of the configurations is given in Table 6.

4.2 MODEL OSCILLATION CONTROL CHECKS

Above moderate angles of attack ($\alpha > 15$ deg for most Mach numbers), the roll balance could not maintain control of the model motion. The control system for the model oscillation uses a closed-loop feedback system with variable-gain feedback referred to as "Summing Amp" in Fig. 10. The roll test was begun with a summing amplifier gain of 5, but during the test, the oscillation amplitude was erratic above moderate angles of attack and additional gain was required to compensate for disturbances. Each time a summing amplifier gain value of 5 was exceeded, the model oscillation frequency changed abruptly to 62 Hz. After the test, a thorough analysis of the system and the model was made to ascertain the source of the control problem and to determine a solution.

To investigate the problem, the system was installed in the laboratory and the effect of summing amplifier gain was studied in the presence of discrete frequencies of noise impressed by a magnetic shaker and the magnetic damper. All of these tests showed that the control was good to a summing amplifier gain of 33 regardless of the impressed frequencies. The obvious conclusion was the existence of a basic difference between the support structures of the laboratory and wind tunnel.

The system was reinstalled in the Tunnel 16T test cart in a configuration identical to the one used in the wind tunnel test (see Fig. 6d). The F-16A model was installed and various configurations of external stores were mounted on the wings for the control checks. Again, the magnetic shaker attached to the sting was used to impress discrete frequency vibration. At summing amplifier gains of 5 or less the model motion was very acceptable; however, when a gain of 5 was exceeded the model motion became distorted by a 62.8-Hz frequency regardless of the impressed frequency of the shaker. At this point, the model and strut assembly continued to oscillate ("buzz") at 62.8 Hz even after the control was shut off. With the external stores and wing tip missiles removed, a summing amplifier gain of 21 was achieved before the buzz frequency was excited. A set of steel wings was temporarily available and was installed with the wing tip missiles. A gain of 21 was obtained with satisfactory model motion. The F-16A model was removed from the balance, and the calibration body installed. A summing amplifier gain of 33 was obtained with no distortion in the forced motion.

A summing amplifier gain of 5 in Tunnel 16T could not be exceeded because the spring-mass system of the combined F-16A model and tunnel support mechanism allowed the support structure to excite the F-16A model wings and set them in motion at the buzz

frequency. Once the wings began to buzz, this frequency was fed through the control loop and eventually back to the torque beam where it was then applied to the model motion. The oscillations were then self-sustaining, and the summing amplifier gain had to be adjusted to zero to extinguish them.

The solution to the control problem for future tests would be to make the F-16A model wings stiffer (an expensive proposition) or to eliminate the mechanical interaction of the support structure with the wing vibration. The study also showed that a stiffer torque beam may be necessary to overcome the disturbances encountered in Tunnel 16T.

Posttest investigation of the roll motion control problem prompted an extensive laboratory and test cart checkout of the P/Y balance system before its test. As before with the roll balance, the use of large summing amplifier gain for the P/Y balance presented no problem in the laboratory regardless of the model configuration or impressed frequencies by the magnetic shaker or magnetic damper. The system was installed in the cart on a much stiffer support system than was used during the roll test (Figs. 6c and d). The magnetic shaker was attached to the model sting just aft of the model or calibration body, and the system was excited at each of the discrete frequencies identified as a natural frequency of some system/support component (see Table 7). The control system usually maintained undistorted model motion for gains up to 20 with either the model with stores or calibration body. It was concluded that the use of large summing amplifier gain for control of model motion during the tests would not be a problem on the P/Y test for either or both of two reasons:

1. The pitch and yaw motion did not excite the wing vibration mode which accompanied the roll control problem.
2. The model support system was substantially different from the one used for the roll test.

Therefore, it was decided to proceed with the wind tunnel tests. The tests were conducted successfully with a control problem at only one high-angle-of-attack condition at one Mach number for yaw oscillation ($\alpha = 50$ deg at Mach 0.4).

4.3 TEST DESCRIPTION

4.3.1 Test Conditions

A summary of the test conditions at each Mach number follows.

<u>M</u>	<u>P_t, psf</u>	<u>T_t, °F</u>	<u>q, psf</u>	<u>p, psf</u>	<u>Re/ft x 10⁻⁶</u>	<u>V, ft/sec</u>
0.2	1976	93	53	1921	1.2	229
0.2	3904	98	106	3797	2.4	230
0.4	2168	110	217	1942	2.4	461
0.6	788	110	155	618	1.2	678
0.6	1560	108	308	1223	2.4	677
0.8	661	110	194	434	1.2	882
0.8	1316	110	386	863	2.4	881
0.9	625	109	209	370	1.2	976
0.9	1253	109	428	741	2.4	976
1.2	588	110	244	243	1.2	1237
1.4	1170	100	504	367	2.4	1376

A test summary showing all configurations that were tested is given in Table 8.

4.3.2 Data Acquisition

After tunnel conditions and model attitude were established, the model was brought to the desired oscillation amplitude at the resonant frequency of the model balance system. The system was allowed to stabilize, then data were recorded. Generally three data points at each angle of attack were recorded in the facility computer from the forced-oscillation balance control and oscillation system (FOBCARS). The timewise signal from each data channel was recorded on magnetic digital and analog tapes for analysis after the test.

4.3.3 Data Reduction

The digital readouts of the data acquisition instrumentation from the FOBCARS were input to the facility computer for reducing the data to coefficients. The direct-damping coefficients were obtained using data reduction equations and procedures given in Refs. 5 and 6. The pitch- and yaw-damping results were corrected for sting motion, as discussed in Ref. 7. The cross and cross-coupling data were reduced using equations derived by methods as discussed in Ref. 1.

4.3.4 Uncertainty of Measurements

In general, instrumentation calibrations and data uncertainty estimates were made using methods recognized by the National Bureau of Standards (NBS) (Ref. 8). Measurement

uncertainty is a combination of bias and precision errors defined as:

$$U = \pm (B + t_{95}S)$$

where B is the bias limit, S is the sample standard deviation, and t_{95} is the 95th percentile point for the two-tailed Student's "t" distribution, which for degrees of freedom greater than 30 equals 2.

Estimates of the measured data uncertainties for this test are given in Tables 9a and b. The balance data uncertainties were determined from in-place static and dynamic calibrations through the data recording system and data reduction program. Static load hangings on the balance simulated the range of loads and center-of-pressure locations anticipated during the test, and measurement errors were based on differences between applied loads and corresponding values calculated from the balance equations used in the data reduction. Load hangings to verify the balance calibration were made in-place on the assembled model. Static and dynamic calibrations of the dynamic stability balance system allowed the measurement uncertainty to be that attributable to the amount of nonrepeatability of the calibration constants. The sting and parts of the balance not dynamically calibrated were calibrated by static load hangings over the range of anticipated loads. Uncertainties in the measurements of sting effects were included in the error analysis. Structural damping values were obtained at near-vacuum conditions before the tunnel flow was started to evaluate the still-air damping contribution.

Propagation of the bias and precision errors of measured data through the data reduction equations was made in accordance with Ref. 8 and the results are given in Table 9c. The uncertainties are for steady-state conditions. Occasionally vibration and noise of the wind tunnel environment caused the scatter in the data to exceed the estimated uncertainty.

The uncertainties in the cross and cross-coupling results were generally large compared to the measured levels and must be decreased. Low signal output and uncertainties of the basic measurements from the balance, and sting-bending effects were the primary factors in the uncertainties. The propagation of errors from the basic measurements is inversely proportional to the oscillation amplitude, whereas the level of the primary balance outputs is directly proportional to the oscillation amplitude. Operation at larger amplitudes would decrease the uncertainties. Further improvement could be obtained by increasing the system sensitivity to the measured loads by using higher gain amplifiers and a finer resolution analog-to-digital converter. Additional reduction in the uncertainty could be obtained by using stiffer stings to reduce the sting-bending effects.

4.4 RESULTS AND DISCUSSION

The results of the pitch, yaw, and roll test phases are presented in Figs. 11 through 17. Digital Datcom predictions (Ref. 9) are compared to the results.

The normal-force data from the can balance are illustrated in Fig. 11 for three Mach numbers. The theory, Ref. 9, generally agrees with the data. The data are generally repeatable within ± 0.01 and are unaffected by forced model oscillation either in pitch or yaw.

Typical longitudinal stability results for clean wing configuration, i.e., no external stores, are presented in Fig. 12 at Mach numbers 0.2 and 0.8. The results indicate very small effects of stabilator deflection on the derivatives. The agreement in C_{m_α} and $C_{m_q} + C_{m_{\dot{\alpha}}}$ between the P/Y and can balances is less than the estimated uncertainty (Table 9c). The pitching moment from can balance measurements seems to be biased approximately -0.02 compared to the results from the P/Y balance. The bias was probably caused by an axial-force interaction. The theory, Ref. 9, does not predict the levels or trends in the data.

Lateral stability results are shown in Fig. 13 for Mach number 0.2. Stabilator deflection had little effect on the yaw results. There is very good agreement in C_n between the can and P/Y balances. Unfortunately, the rolling-moment gages had broken before the yaw data were obtained, and the derivative results from the can balance were invalid. The theory, Ref. 9, agrees better at low angles of attack ($\alpha < 15$ deg) with the yawing lateral stability results than it does with the longitudinal stability results.

The effects of external stores on the basic damping derivatives are illustrated in Fig. 14. In general, the effects were small for all test conditions.

The damping derivatives are shown in Fig. 15 for the Mach numbers of the tests at representative angles of attack. The model exhibited slight dynamic lateral instability at high angles of attack at high transonic Mach numbers. In general, longitudinal stability increased with increasing angle of attack at each Mach number. The roll stability was not significantly affected by Mach number.

A comparison of the static yawing-moment derivative, $C_{n\dot{\beta}} \sin \alpha$, is made in Fig. 16 for the roll and P/Y balances. The comparison of the data from the two balances substantiates the abilities of the balances to resolve small aerodynamic loads.

Most of the cross and cross-coupling capability was eliminated by the failure of the can balance rolling-moment load cells. The derivatives that were measured were usually very small compared to the uncertainties of the measurements except for $C_{l_{\alpha}}$ and $C_{l_q} + C_{l_{\dot{\alpha}}}$ at low Mach numbers. The measured cross and cross-coupling derivatives are shown in Fig. 17 at Mach number 0.2. These data are not corrected for magnification and phase shift because of the effect of aerodynamic damping on the phase shift. These data are the first such results obtained from tests at AEDC. At present there are no known ways to validate these results.

5.0 SUMMARY

In the early 1970's, AEDC recognized a need for dynamic stability test mechanisms that could obtain a complete set of static and dynamic data. Three balances were designed to perform pitch-, yaw- and roll-oscillation dynamic stability tests to obtain not only the direct derivative data but also attempt to measure the cross and cross-coupling derivatives.

Extensive laboratory investigations of the static and dynamic response characteristics of the balances were performed, and wind tunnel tests were conducted on an F-16A model in Tunnel 16T. Those efforts have shown that the 4,000-lb P/Y balance is operational for testing to high angles of attack ($\alpha \leq 50$ deg) and the roll balance is operational for low angles of attack ($\alpha \leq 15$ deg). (Higher angles of attack might have been possible with stiffer wings.) Furthermore, the results show the following:

1. The can balance results agreed with the P/Y balance where comparisons were possible, both in the laboratory and wind tunnel.
2. Laboratory loadings indicated that the rolling-moment load elements of the can balance had a low natural frequency which caused significant magnification and phase shifts to occur at the planned oscillation rate.
3. The low natural frequency of the rolling-moment load elements of the can balance was excited during the wind tunnel test, causing a failure of the roll elements after several hours of testing.
4. The uncertainties in the cross and cross-coupling derivatives were usually very large compared to the measured results, except for $C_{l_{\alpha}}$ and $C_{l_q} + C_{l_{\dot{\alpha}}}$.
5. The roll dynamic balance experienced control problems above moderate angles of attack at transonic and supersonic Mach numbers.

6.0 RECOMMENDATIONS

This study has indicated that the following steps should be taken with respect to future cross and cross-coupling balance development:

1. The natural frequencies of the load measuring elements must be increased to at least 70 Hz to decrease:
 - a. high dynamics which could cause failure, and
 - b. magnification and phase shift effects.
2. Estimated uncertainties in the cross and cross-coupling data must be reduced. Possible means to do so would be by combinations of the following options:
 - a. operating at higher oscillation amplitudes;
 - b. reducing the uncertainties in the basic measurements by increasing the sensitivity of the system; and
 - c. making the stings stiffer to reduce sting oscillation effects.
3. The can-type balance concept must be analyzed to minimize the diameter of the balance for the high-load capability.
4. The torque beam of the roll balance will need to be strengthened for operation at high angles of attack.

REFERENCES

1. Orlik-Rukemann, K. J., Hanff, E. S. and Laberge, J. G. "Direct and Cross-Coupling Subsonic Moment Derivatives Due to Oscillatory Pitching and Yawing of an Aircraft-Like Model at Angles of Attack up to 40° in Ames 6' x 6' Wind Tunnel." National Aeronautical Establishment LTR-UA-38, November 1976.
2. "Technical Evaluation Report on the Fluid Dynamics Panel Symposium on Dynamic Stability Parameters." AGARD-AR-137, April 1979.
3. Thomson, W. T. *Mechanical Vibrations*. Second edition. Prentice Hall, New York, 1948.
4. *Test Facilities Handbook*. Eleventh Edition. "Propulsion Wind Tunnel Facility, Vol. 4," Arnold Engineering Development Center, June 1979.
5. Riddle, C. D. "A Description of a Forced-Oscillation Balance," AEDC-TDR-62-68 (AD276105), May 1962.

6. Schueler, C. J., Ward, L. K., and Hodapp, A. E., Jr. "Techniques for Measurement of Dynamic Stability Derivatives in Ground Test Facilities." Agardograph 121 (AD669227), October 1967.
7. Burt, G. E. and Uselton, J. C. "Effects of Sting Oscillation on Measurements of Dynamic Stability Derivatives in Pitch and Yaw," Presented at the AIAA 8th Aerodynamics Testing Conference, Bethesda, Maryland, July 8 - 10, 1974.
8. Thompson, J. W. and Abernethy, R. B. et al. "Handbook Uncertainty in Gas Turbine Measurements." AEDC-TR-73-5 (AD755356), February 1973.
9. Finck, R. D., principal investigator. "USAF Stability and Control Datcom," Flight Control Division, Air Force Dynamics Laboratory, Wright-Patterson Air Force Base, Ohio. Revised January 1975.

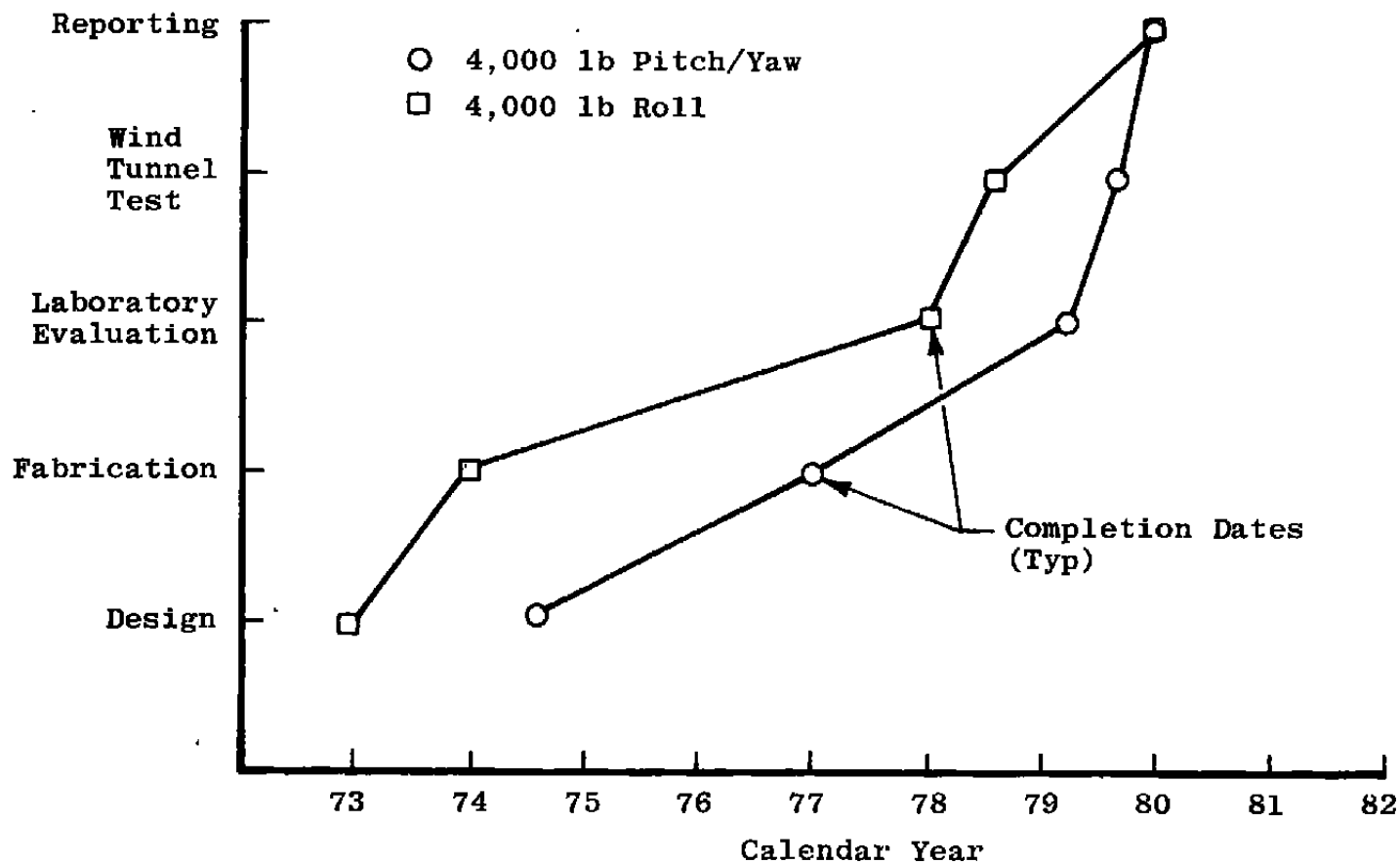
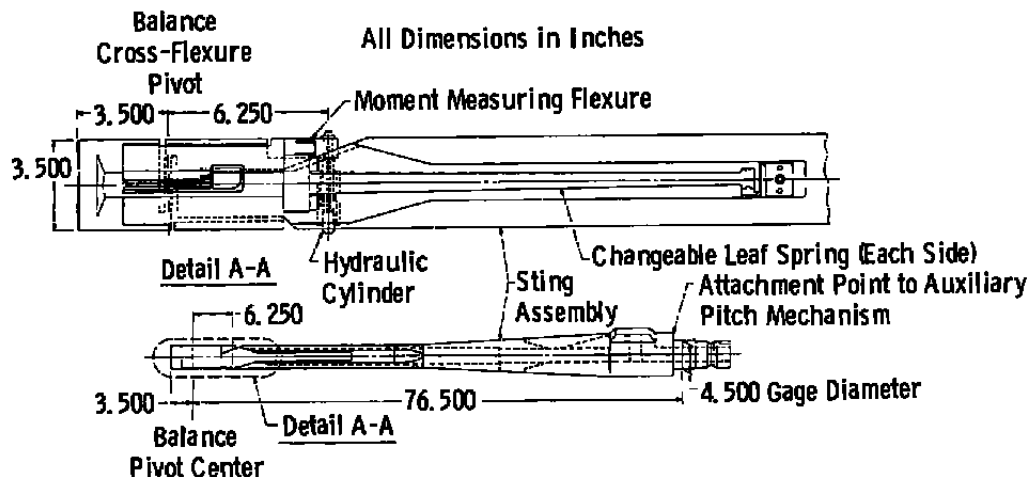


Figure 1. History of 4,000-lb mechanism development.

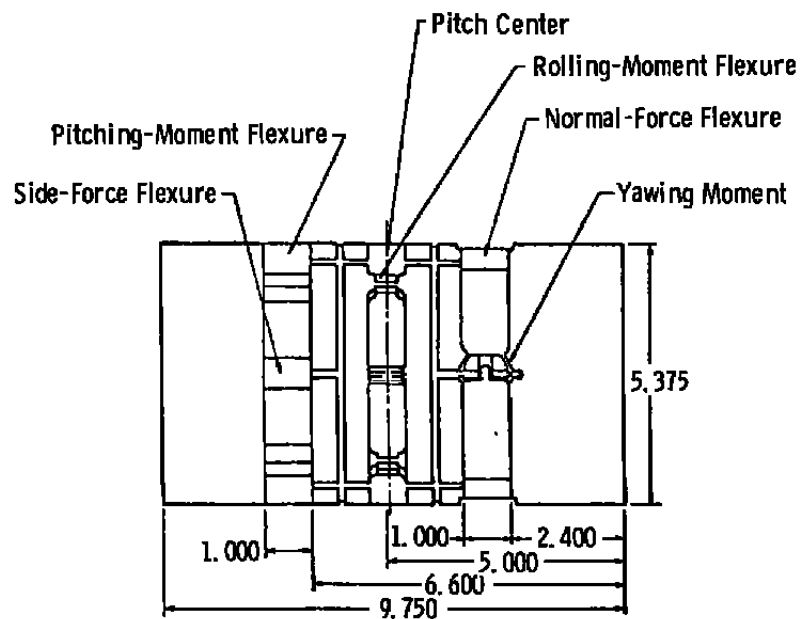


Balance Limits		
Parameter	Pitch Derivative	Yaw Derivative
Normal Force	4,000 lb	3,000 lb
Pitching Moment	$\bar{\theta}_T \times M\theta F$	3,000 in. -lb
Side Force	400 lb	200 lb
Yawing Moment	1,200 in. -lb	$\bar{\theta}_T \times M\theta F$
Rolling Moment	500 in. -lb	500 in. -lb
Axial Force	1,000 lb	
Balance Restoring Spring	1,500 in. -lb/deg	
	9,000 in. -lb/deg	
Total Oscillating Angle	± 2 deg	± 1 deg*
Maximum Frequency	10 Hz	
Torque Drive	300 in. -lb	
	600 in. -lb	

$\bar{\theta}_T = \bar{\theta}$ - (Oscillation Amplitude)

*Maximum Oscillation Amplitude at Design Limits

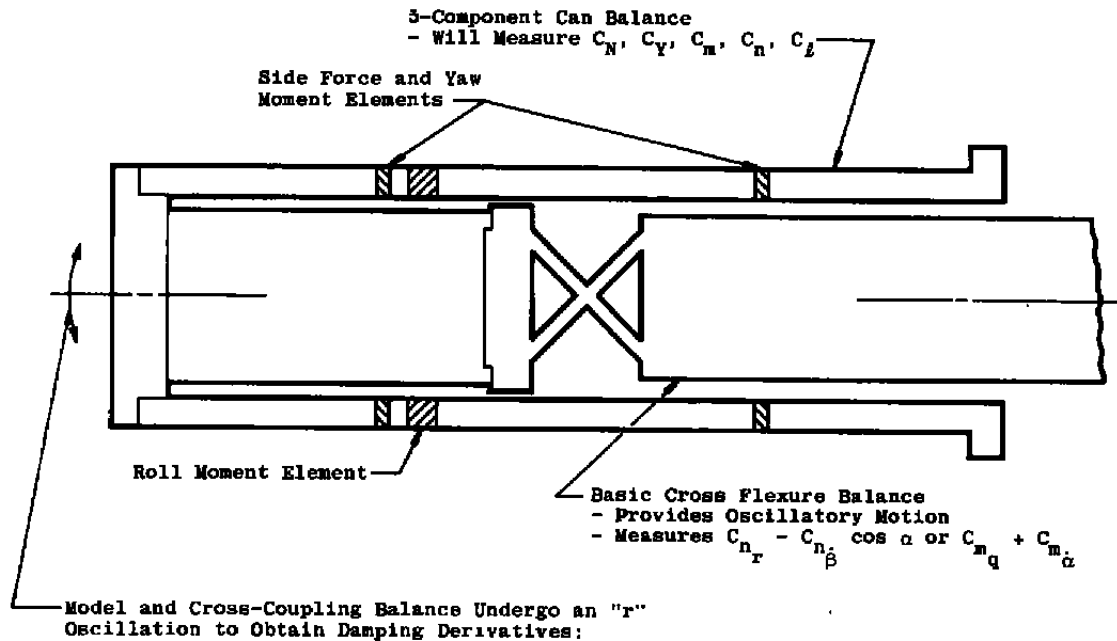
a. 16T/S 4,000-lb pitch/yaw balance
Figure 2. 4,000-lb pitch/yaw balance system.



All Dimensions in Inches

Loads	
Roll	200 in.-lb
N.F.	4,000 lb
S.F.	400 lb
Drag	1,000 lb Not Measured
P.M.	5,600 in.-lb (Includes Spring Constants)
Y.M.	1,250 in.-lb (Includes Spring Constants)

b. 4,000-lb 5-component can balance
Figure 2. Continued.



$$C_{n_r} - C_{n_{\beta}} \cos \alpha, C_{L_r} - C_{L_{\beta}} \cos \alpha, C_{m_r} - C_{m_{\beta}} \cos \alpha$$

$$C_{Y_r} - C_{Y_{\beta}} \cos \alpha$$

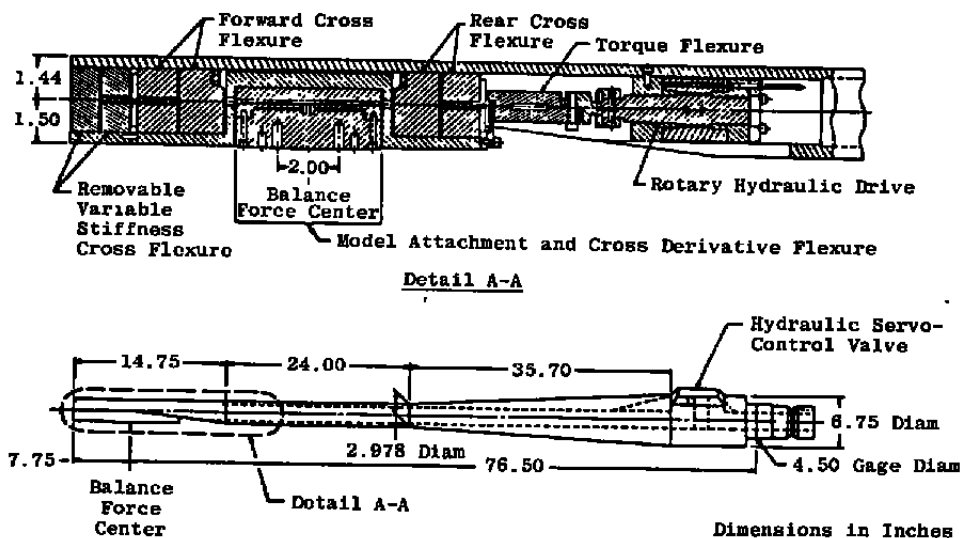
Rotate Flexure 90 deg and Oscillate in Pitch to Obtain:

$$C_{m_q} + C_{m_{\dot{\alpha}}}, C_{L_q} + C_{L_{\dot{\alpha}}}, C_{n_q} + C_{n_{\dot{\alpha}}}$$

$$C_{N_q} + C_{N_{\dot{\alpha}}}$$

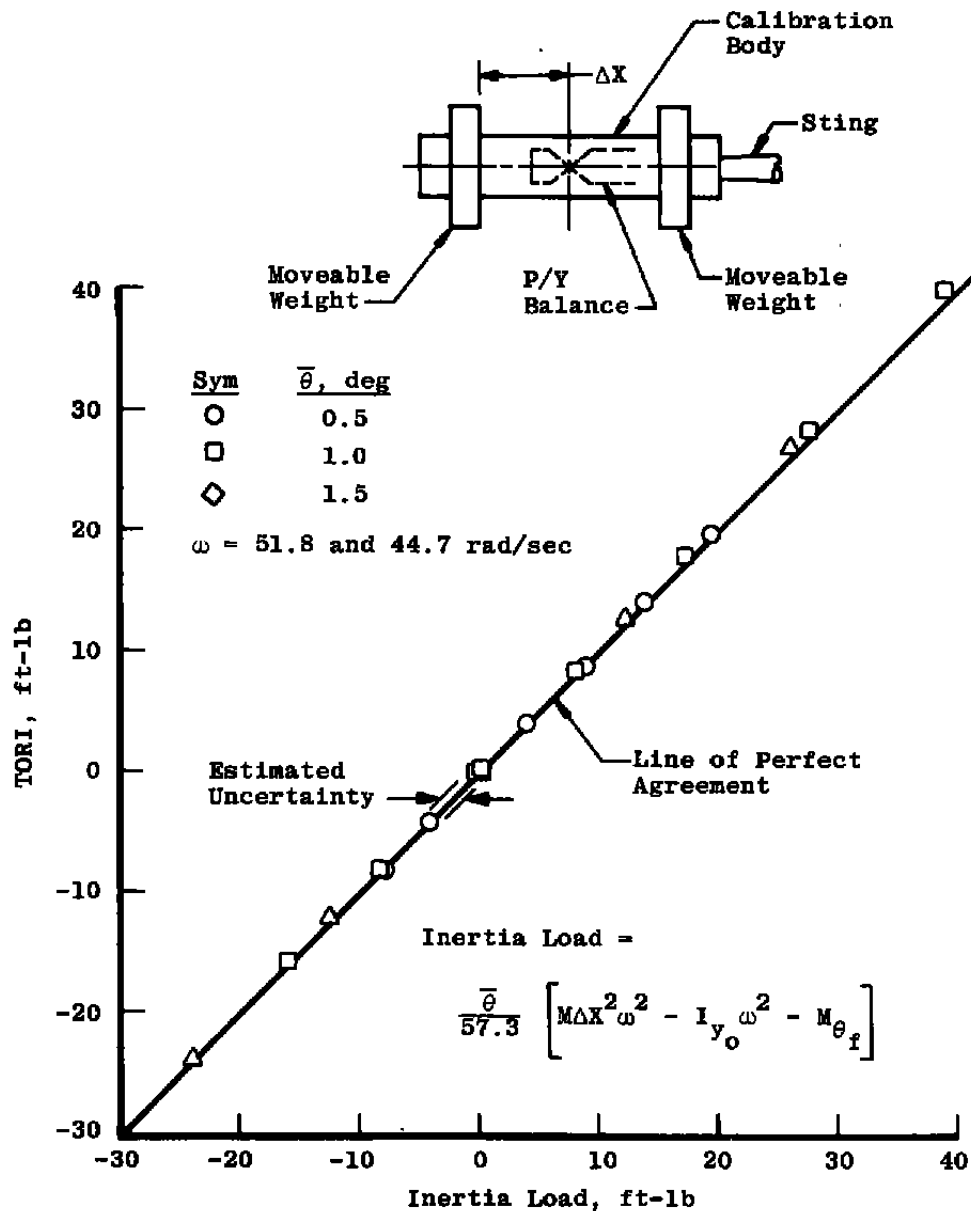
c. Cross and cross-coupling derivative measurement technique

Figure 2. Concluded.



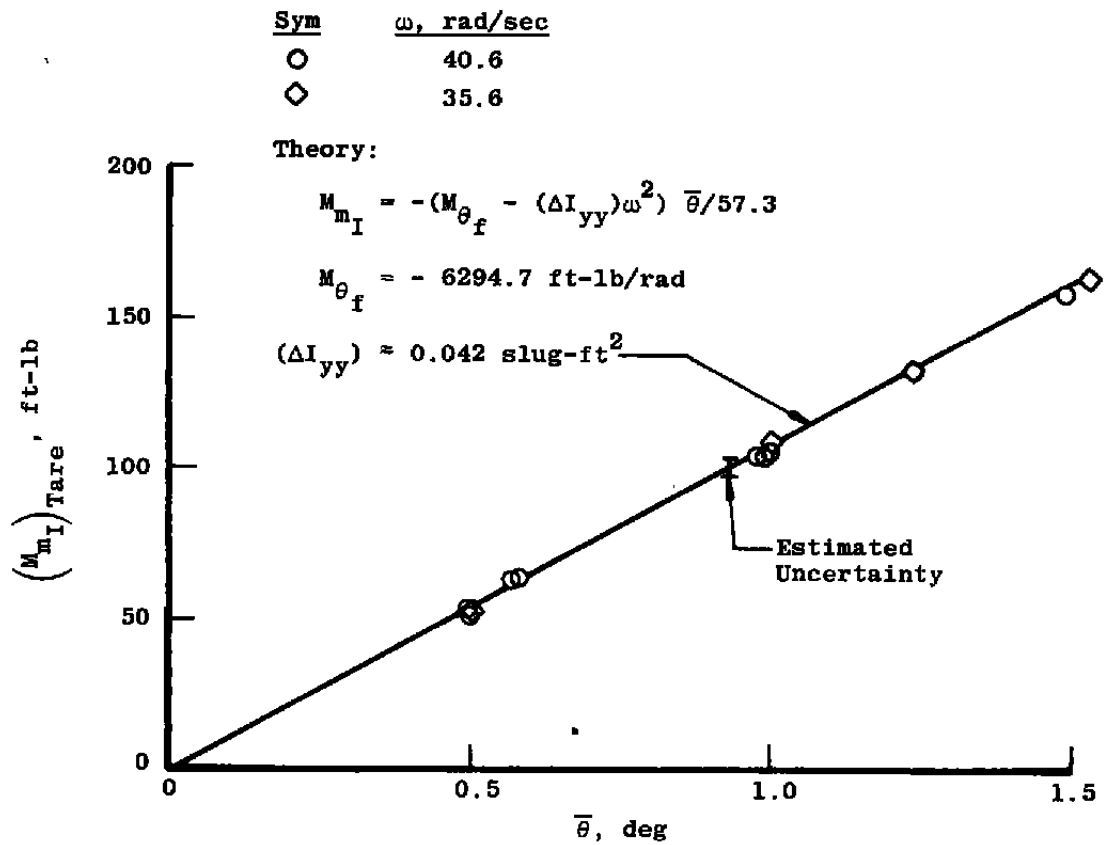
Balance Limits	
Parameter	Roll Derivative
Normal Force	4,000 lb
Pitching Moment	4,000 in.-lb
Side Force	1,000 lb
Yawing Moment	1,000 in.-lb
Axial Force	600 lb
Rolling Moment	615 in.-lb
Cross Flexure Stiffness	308 in.-lb/deg
Variable and Cross Flexure Stiffness	475 in.-lb/deg
Total Oscillating Angle	±2 deg
Maximum Frequency	10 Hz
Torque Drive	200 in.-lb

Figure 3. 4,000-lb roll balance system.

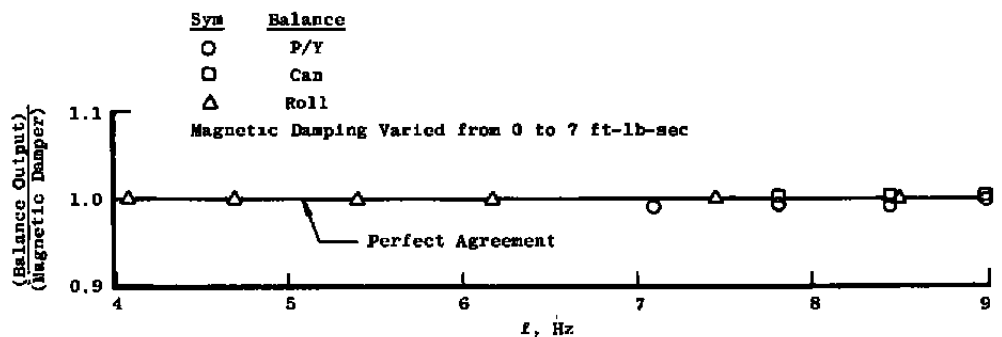


a. P/Y balance

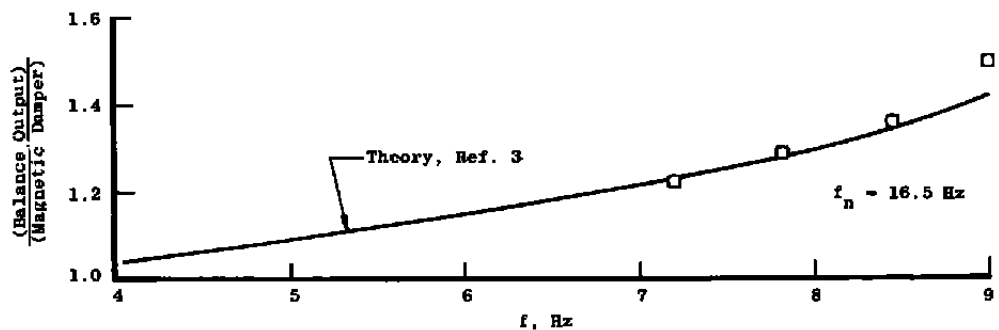
Figure 4. Inertia loading evaluation.



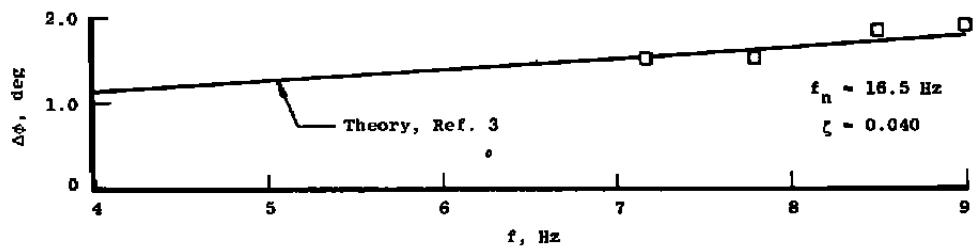
b. Tare-pitching moment, can balance
Figure 4. Concluded.



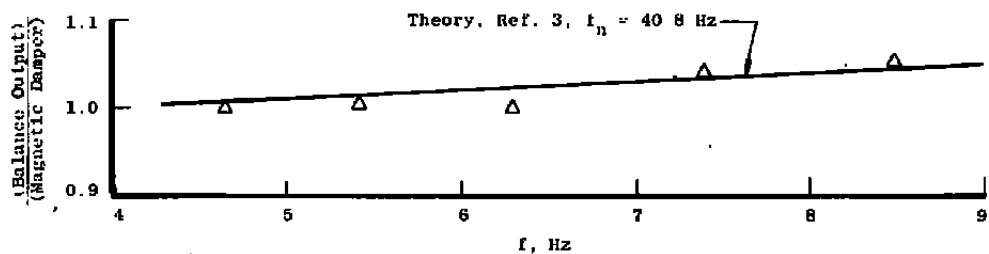
a. Pitching moment



b. Magnification of rolling moment



c. Phase shift of rolling moment



d. Magnification of yawing moment

Figure 5. Frequency effects on balance load-measuring elements.

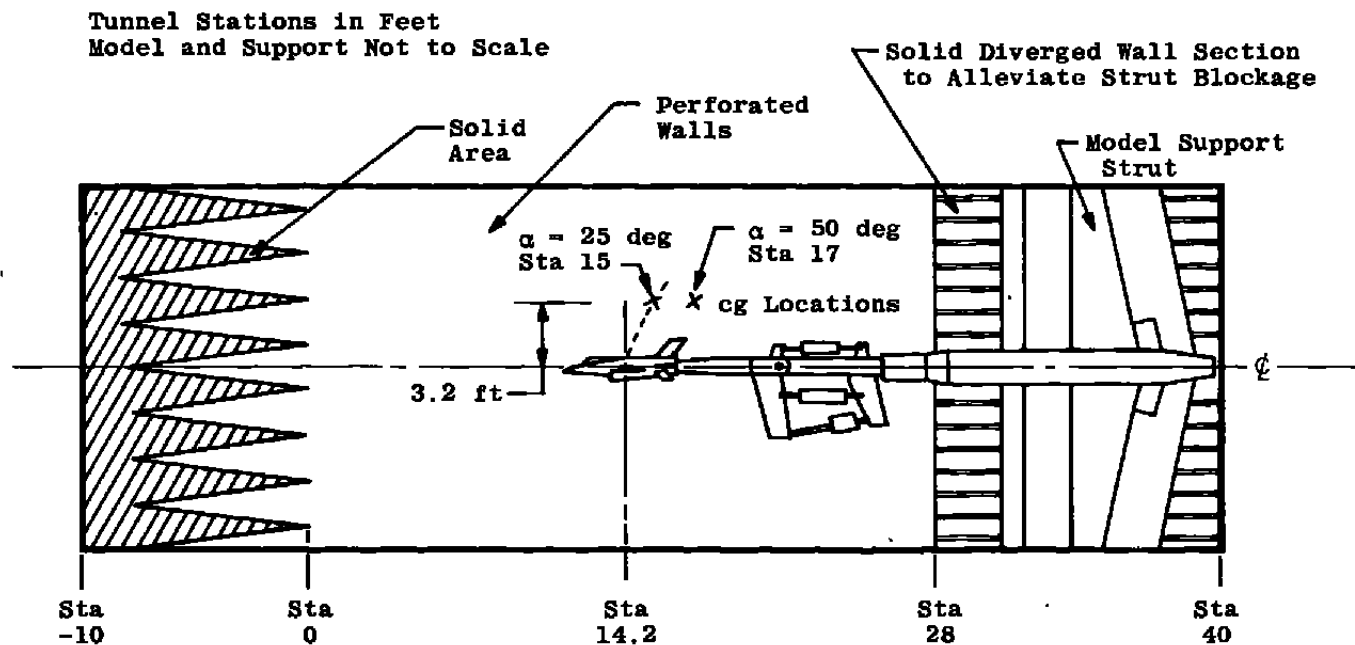
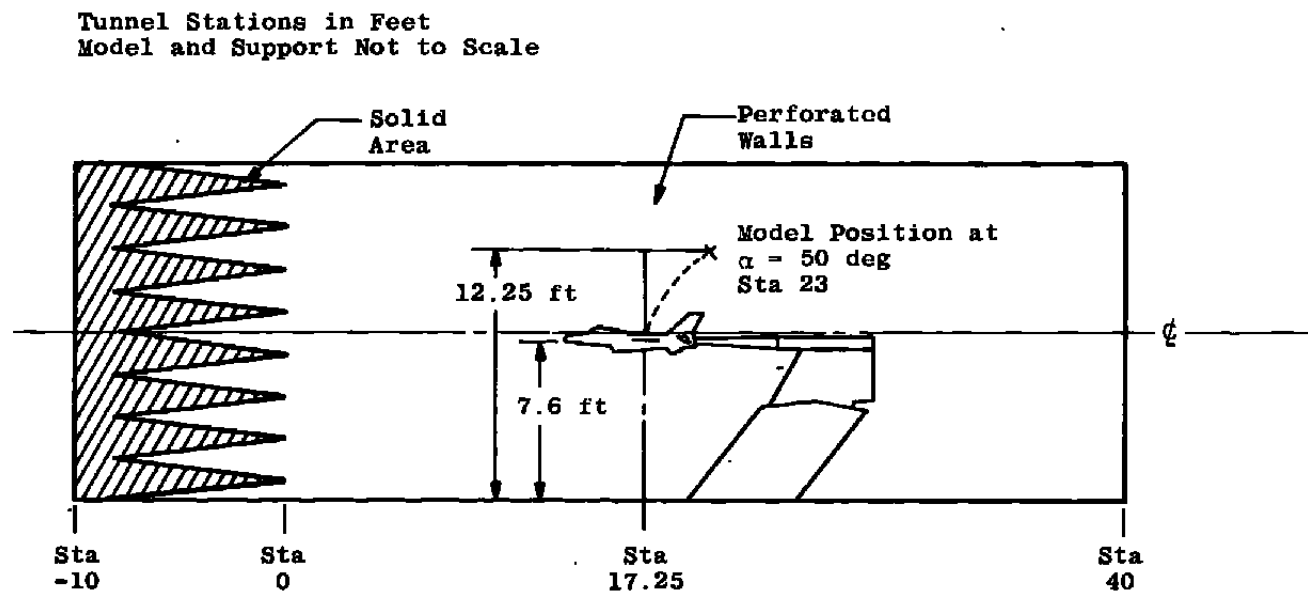
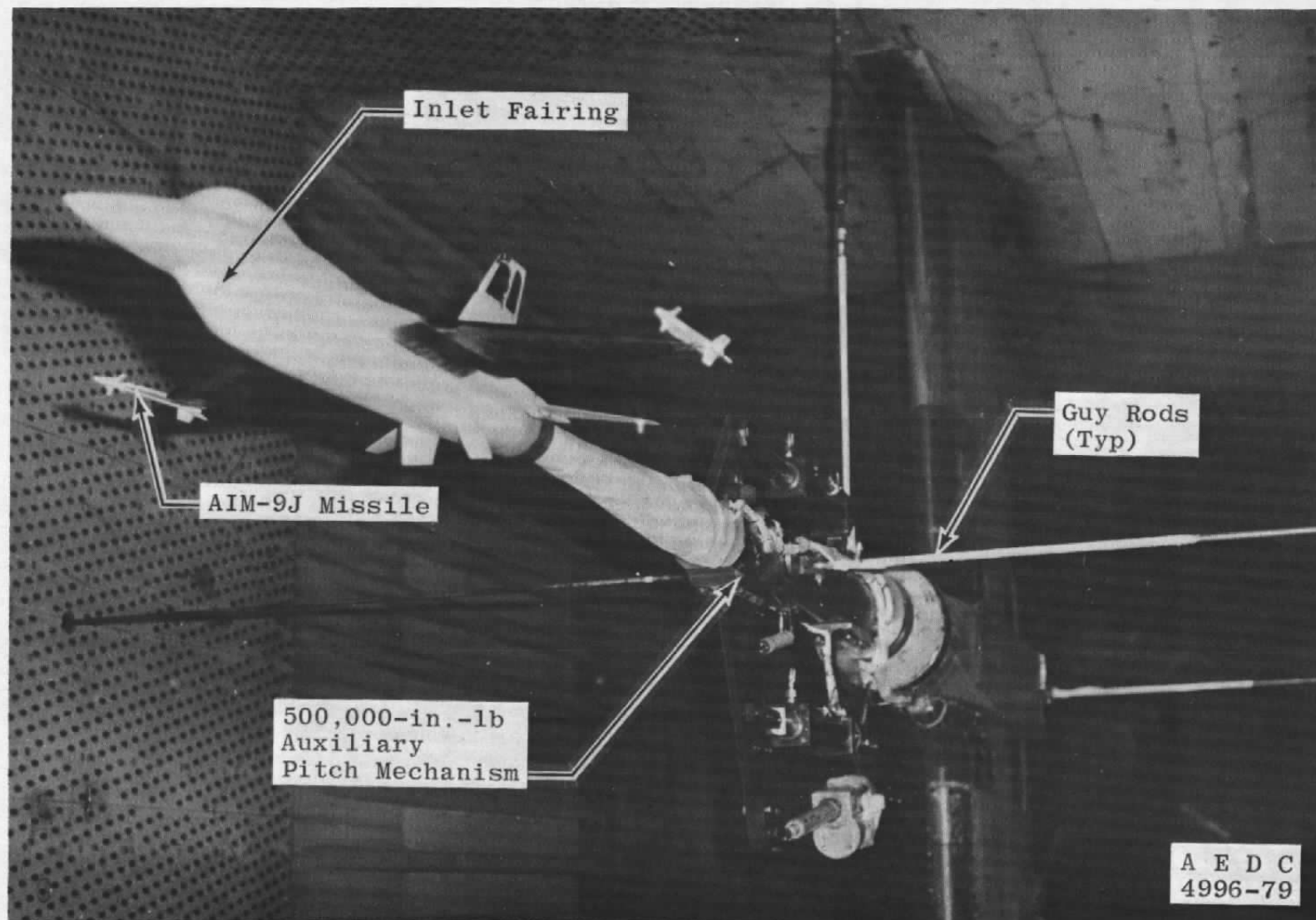


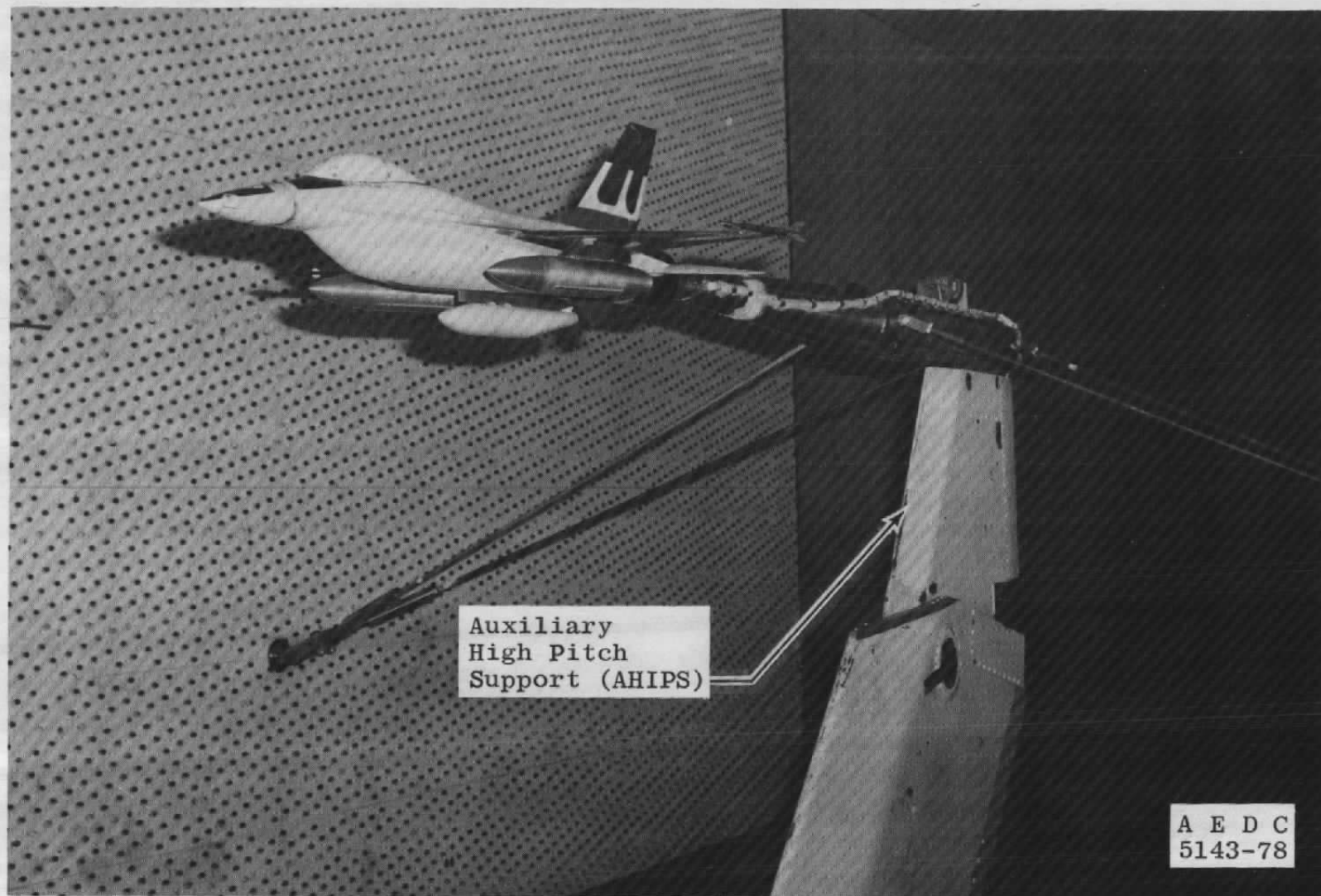
Figure 6. Installation of the models in the Propulsion Wind Tunnel (16T) test section.



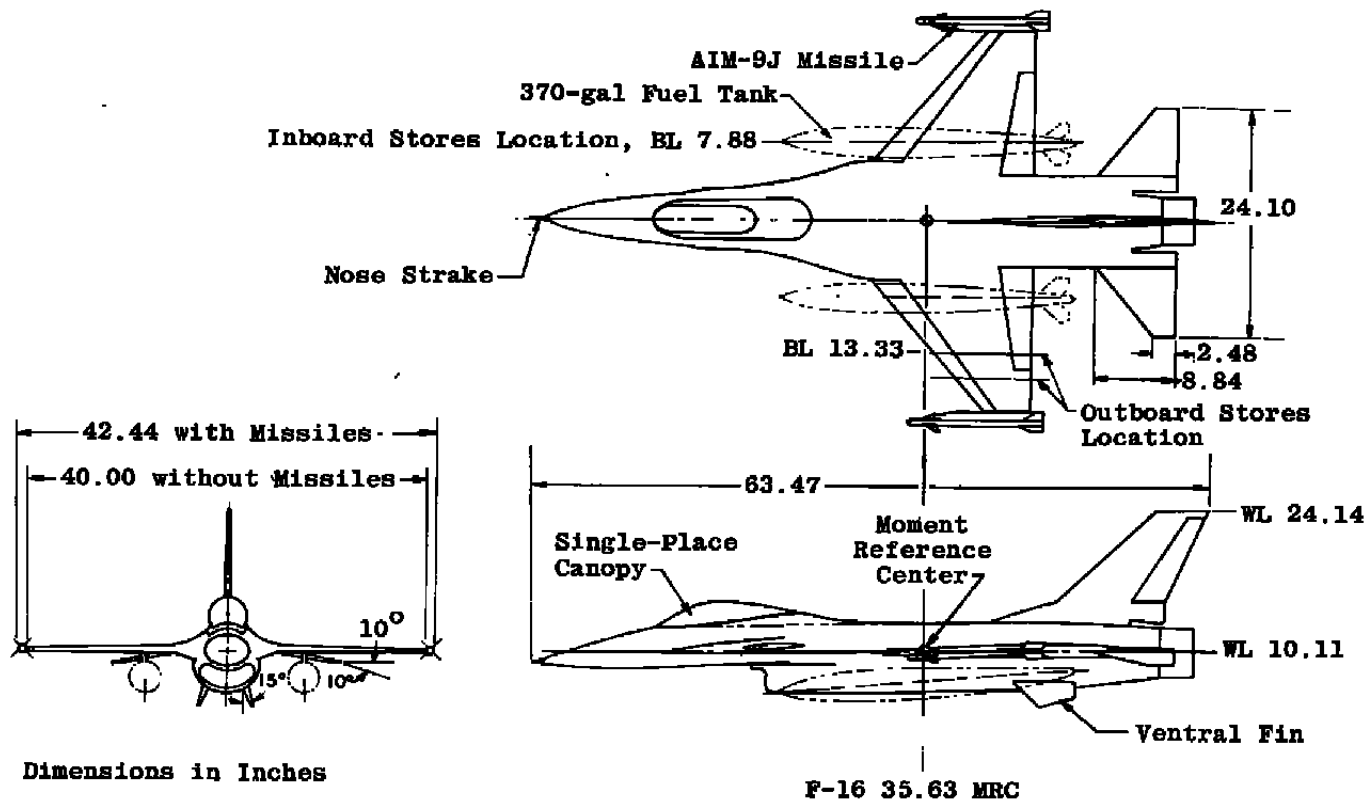
b. Roll test installation
Figure 6. Continued.



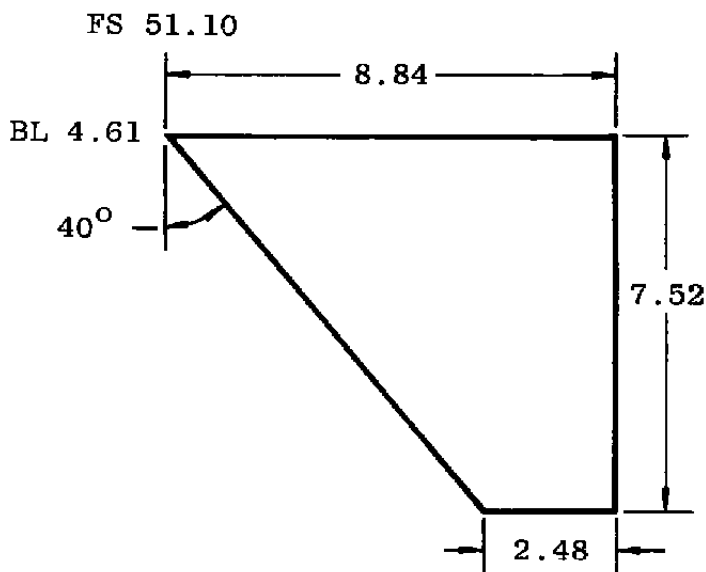
c. Photograph of pitch and yaw test installation, configuration 5
Figure 6. Continued.



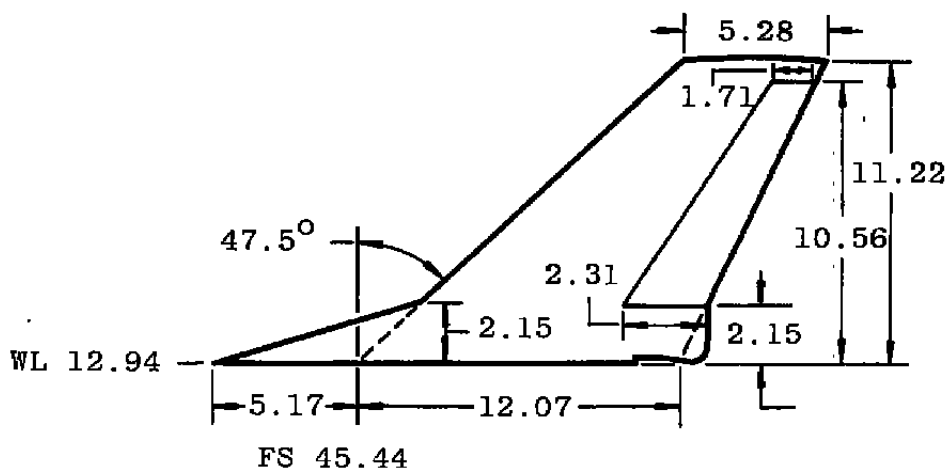
d. Photograph of roll-test installation, configuration 4
Figure 6. Concluded.



a. Overall dimensions
Figure 7. F-16A model details.



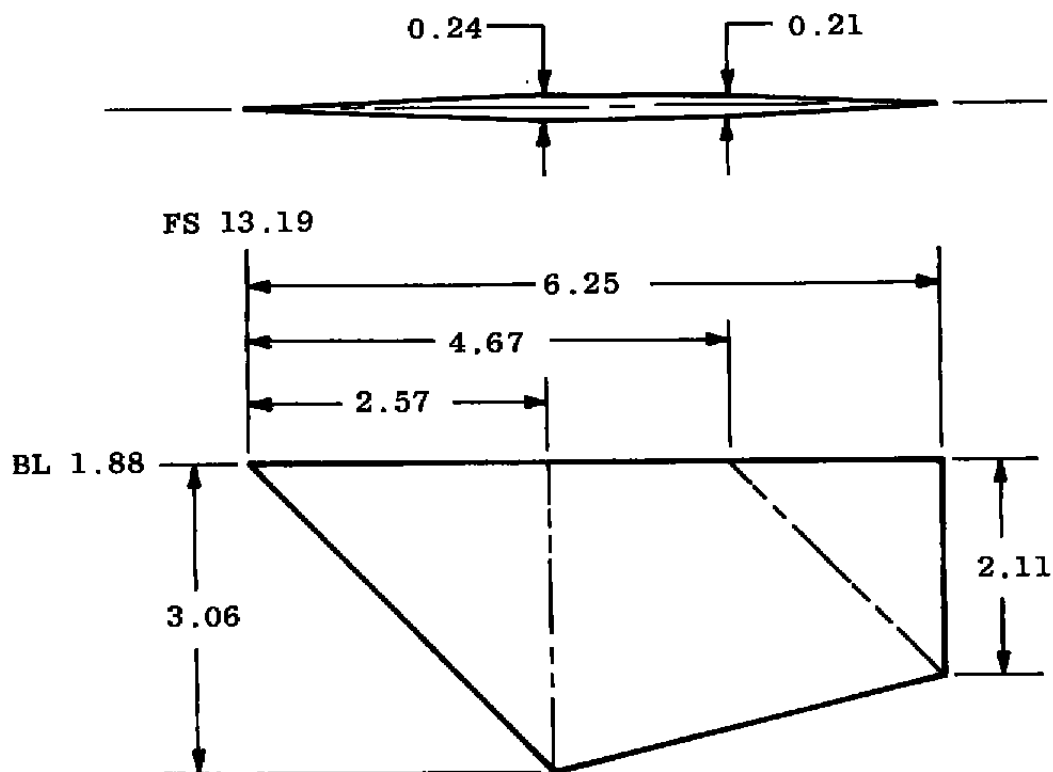
Horizontal Stabilator



Dimensions in Inches

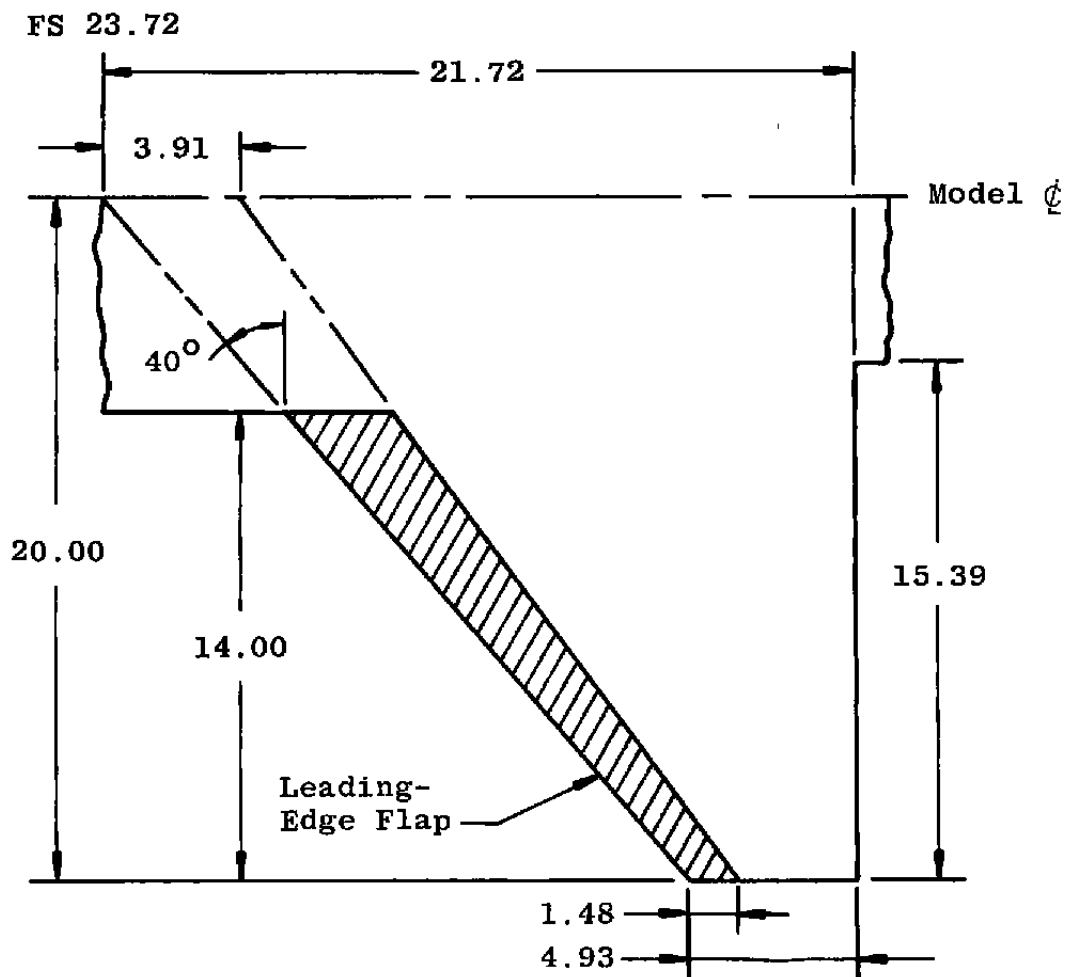
Vertical Stabilizer

b. Tail surfaces
Figure 7. Continued.



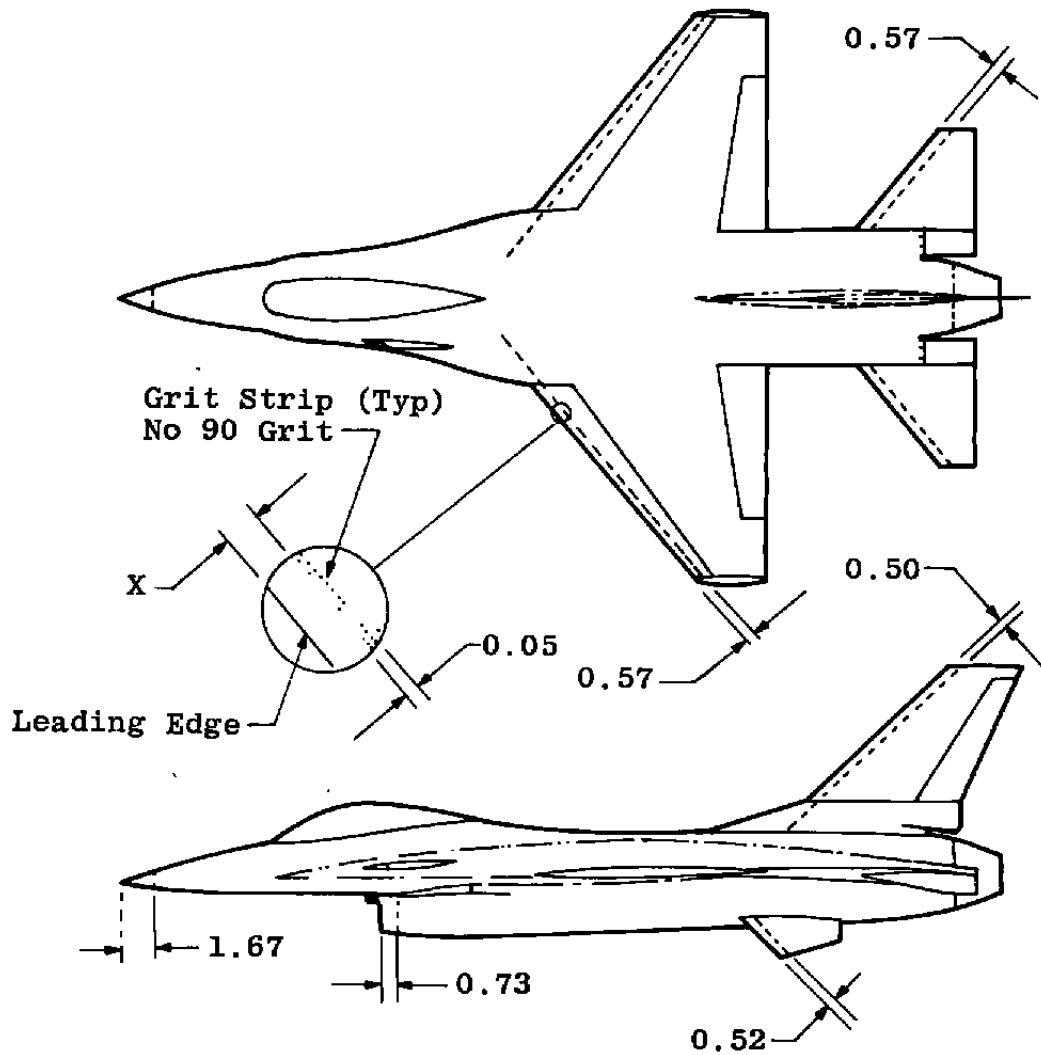
Dimensions in Inches

c. Ventral fin
Figure 7. Continued.



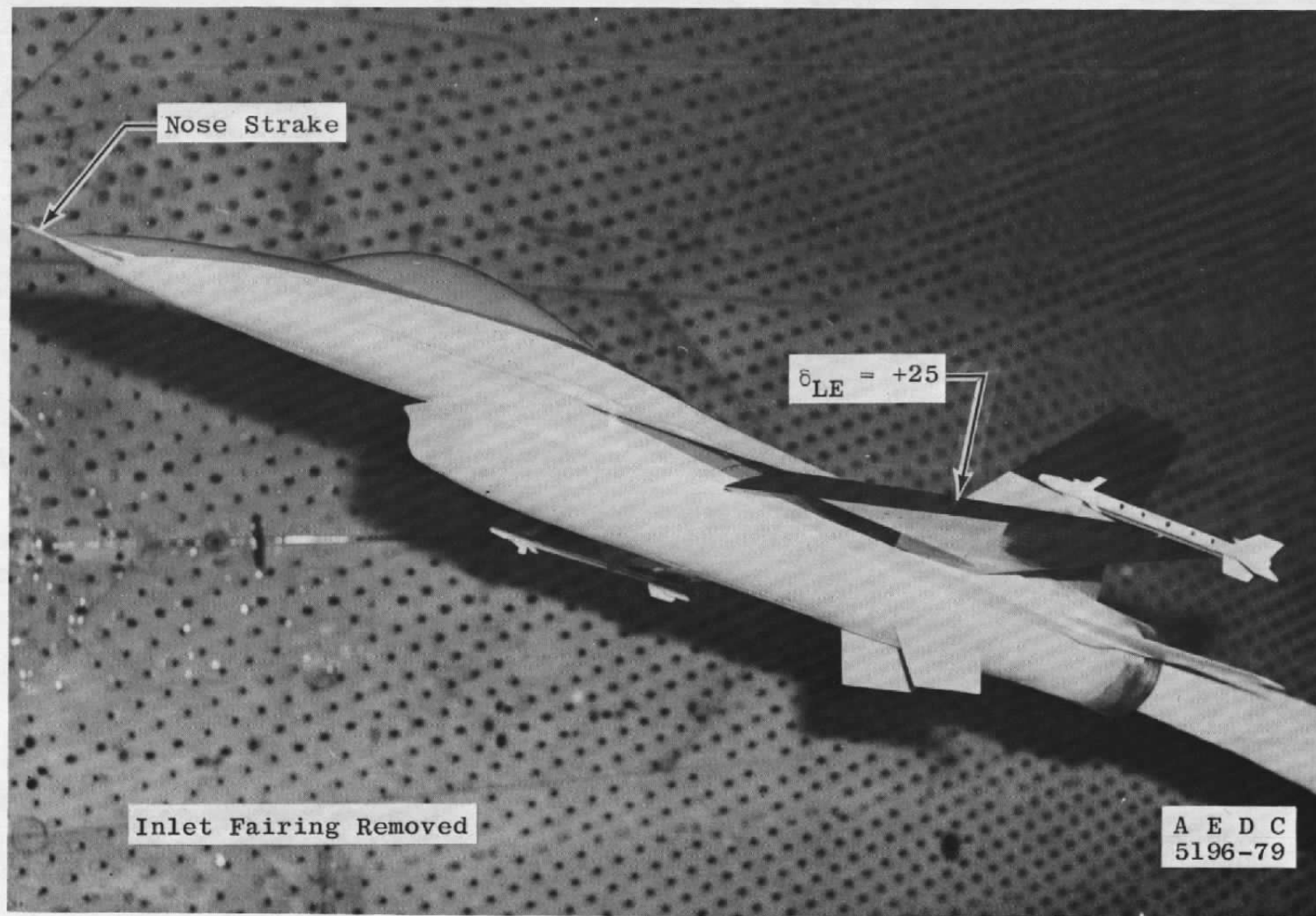
Dimensions in Inches

d. Wing
Figure 7. Continued.



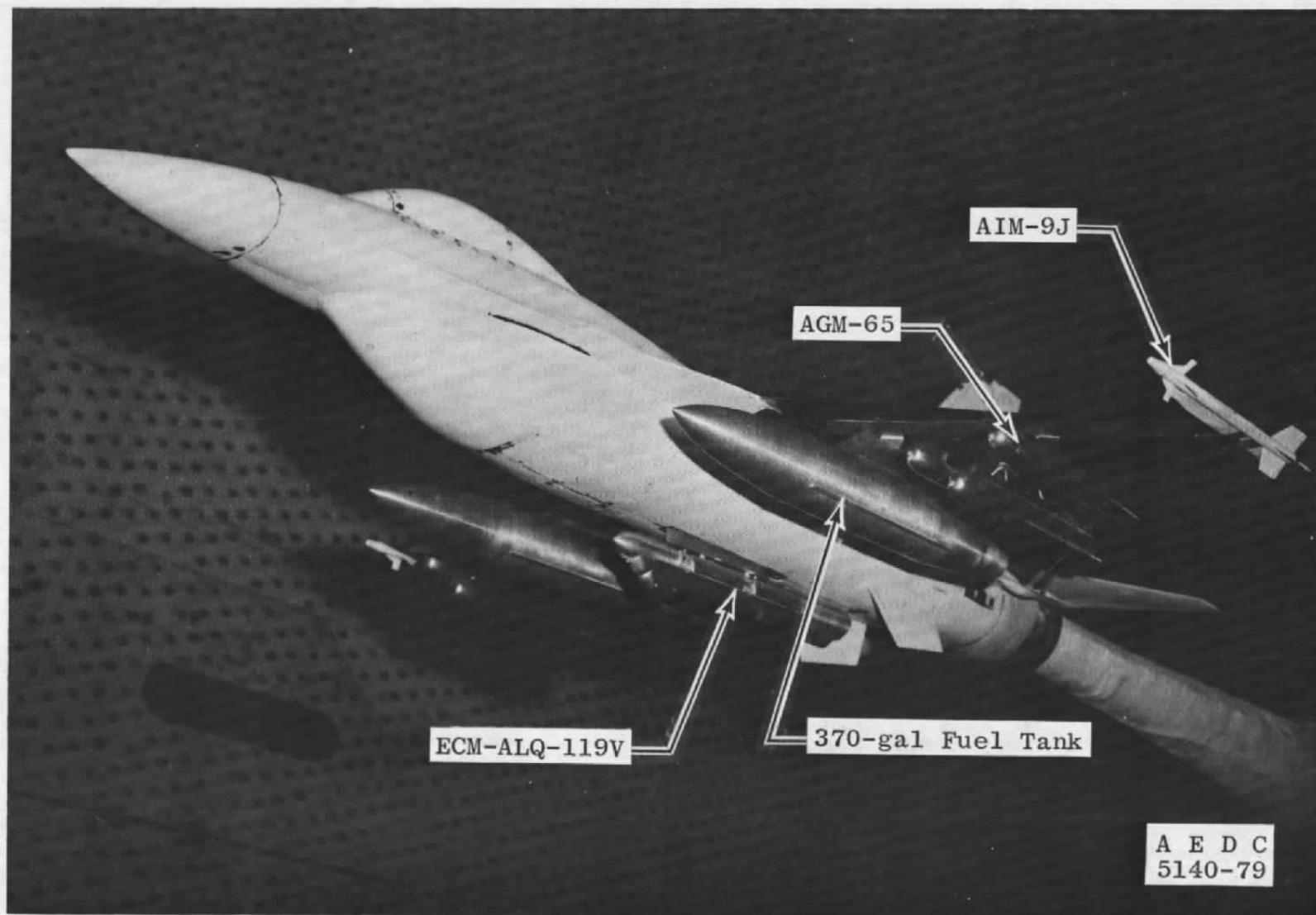
Dimensions in Inches

e. Boundary-layer trip location
Figure 7. Concluded.

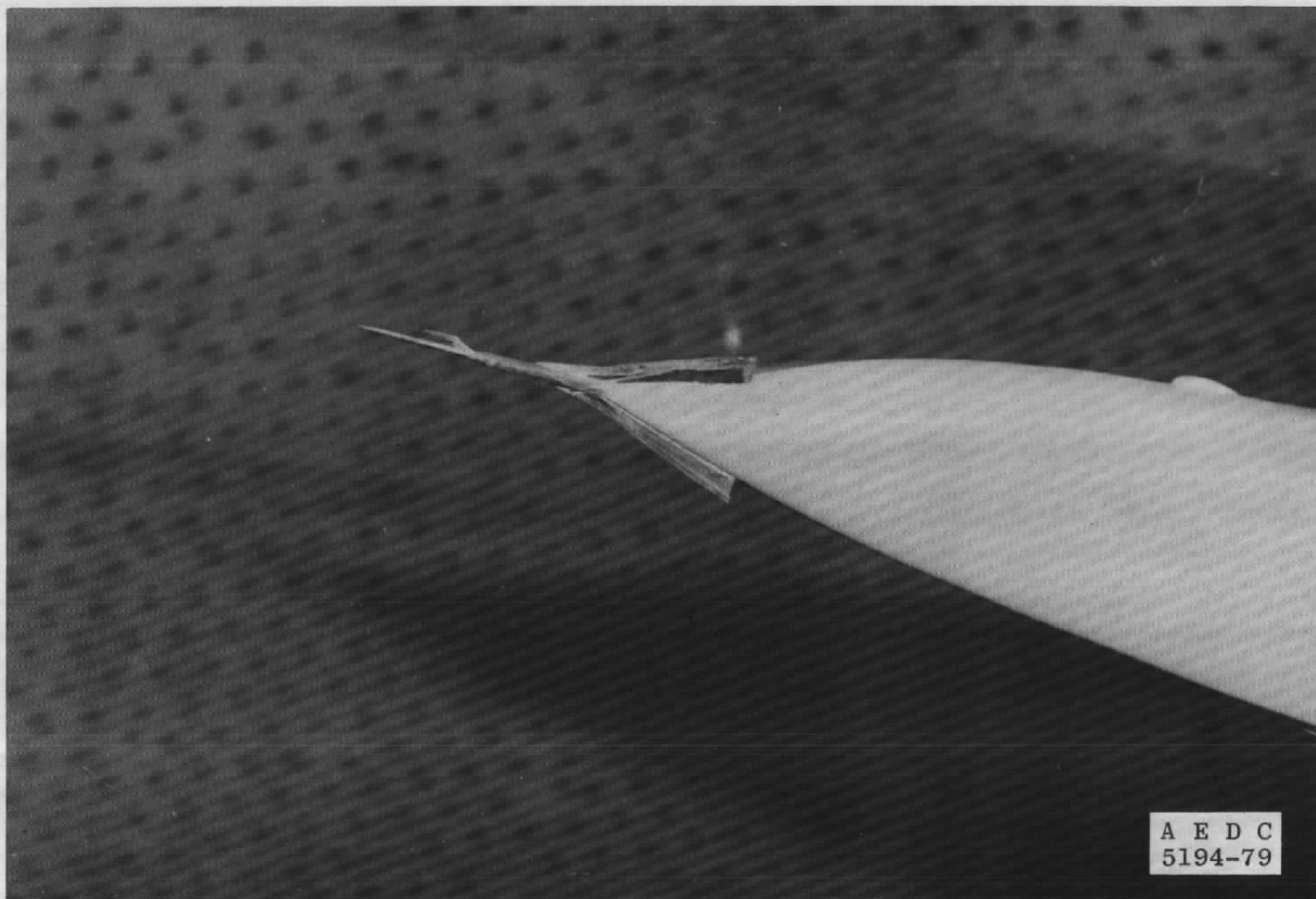


a. Configuration 13

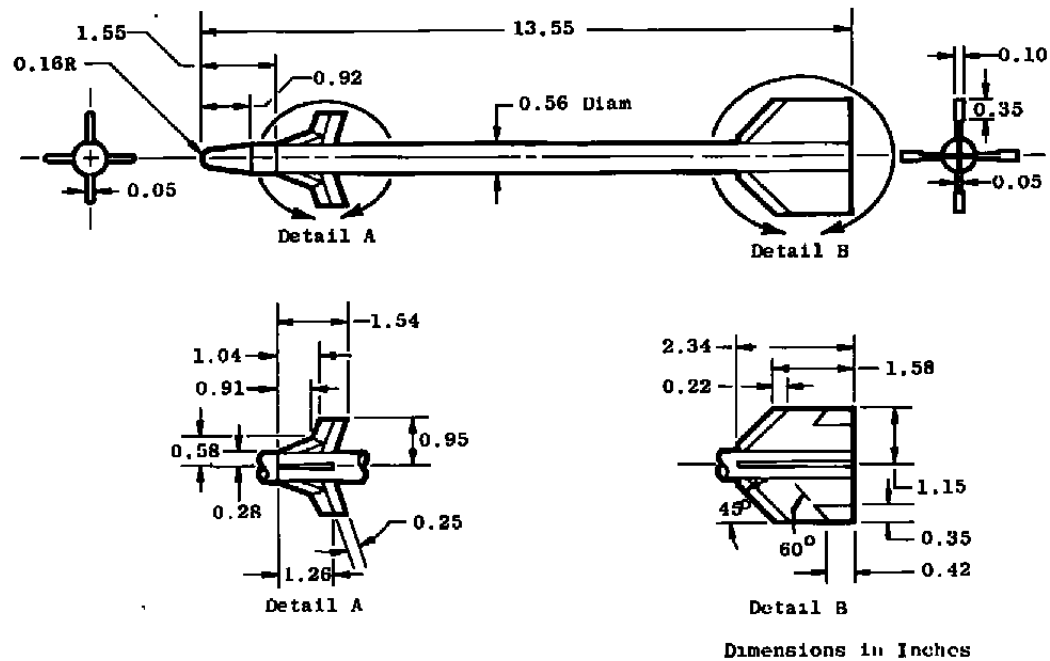
Figure 8. Photographs of typical F-16A configurations.



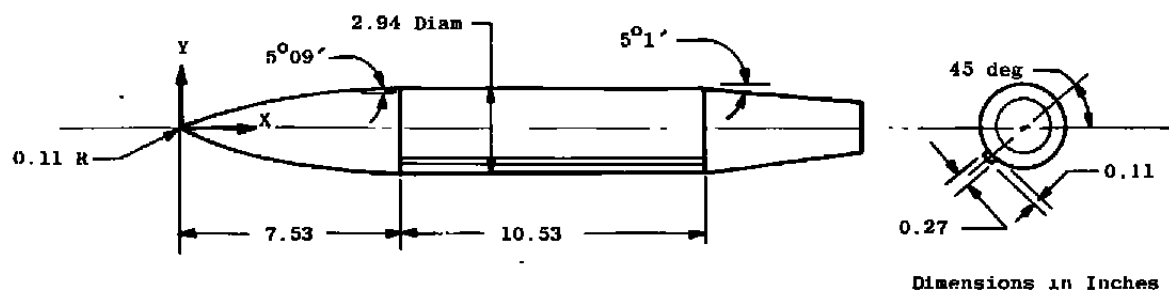
b. Configuration 3
Figure 8. Continued.



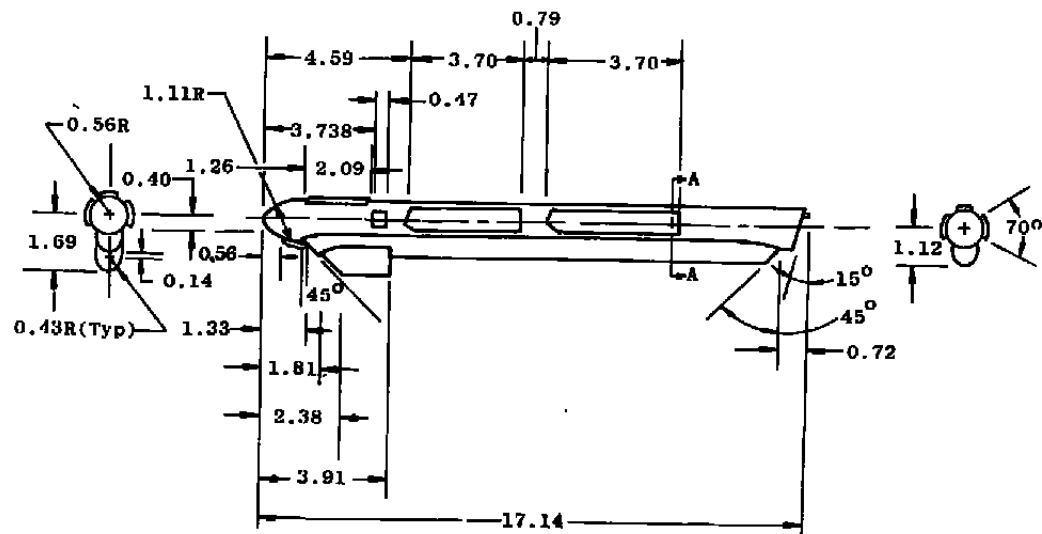
c. Nose strake
Figure 8. Concluded.



a. AIM-9J missile
Figure 9. Details of external stores.

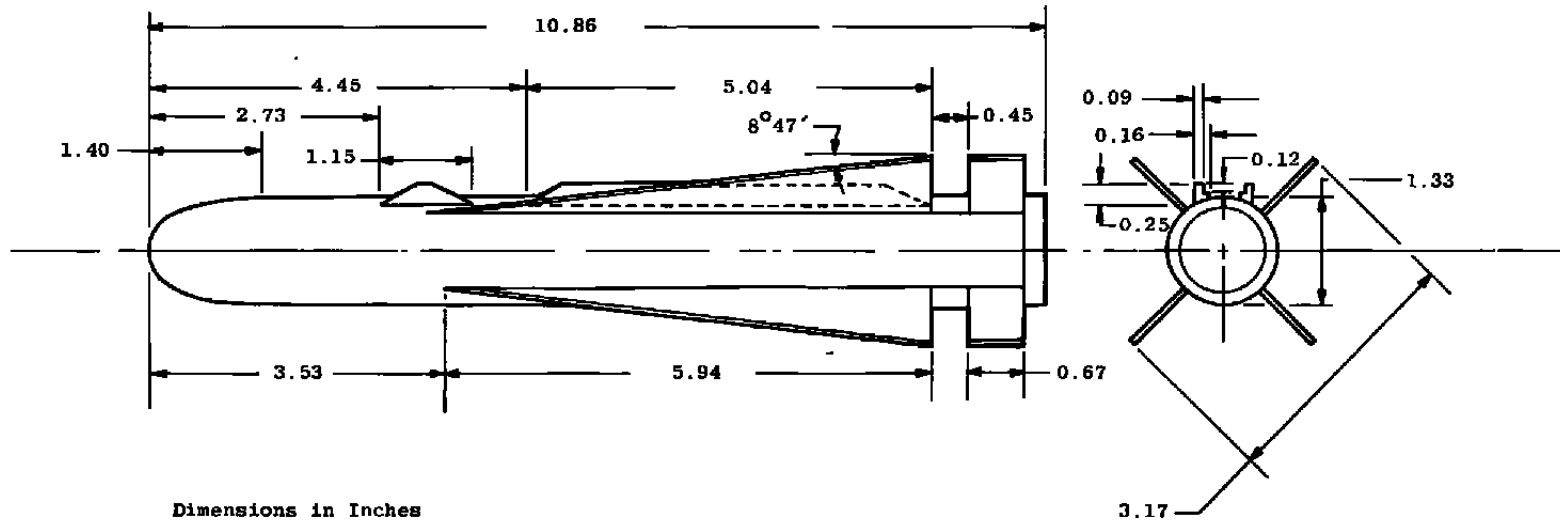


b. 370-gal fuel tank
Figure 9. Continued.

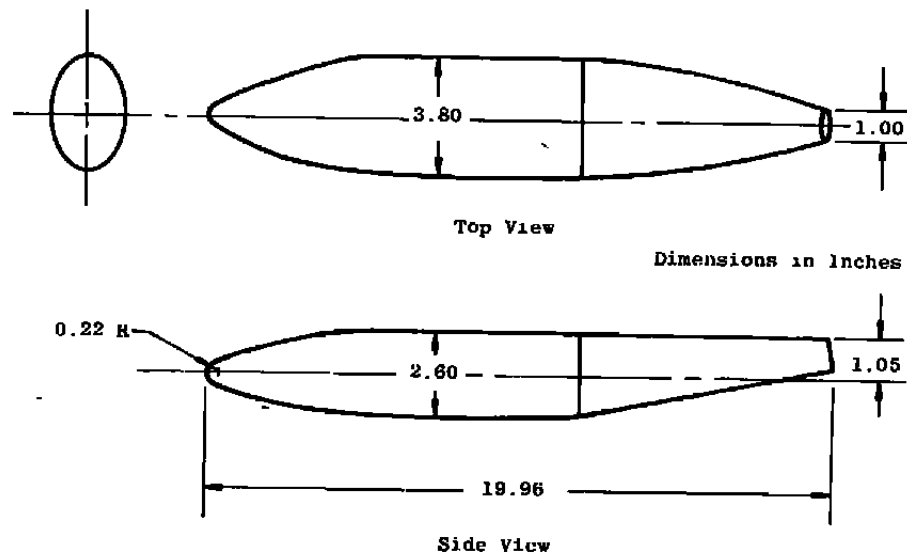


Dimensions in Inches

c. EMC-ALQ-119V
Figure 9. Continued.



d. AGM-65
Figure 9. Continued.



e. 300-gal tank
Figure 9. Concluded.

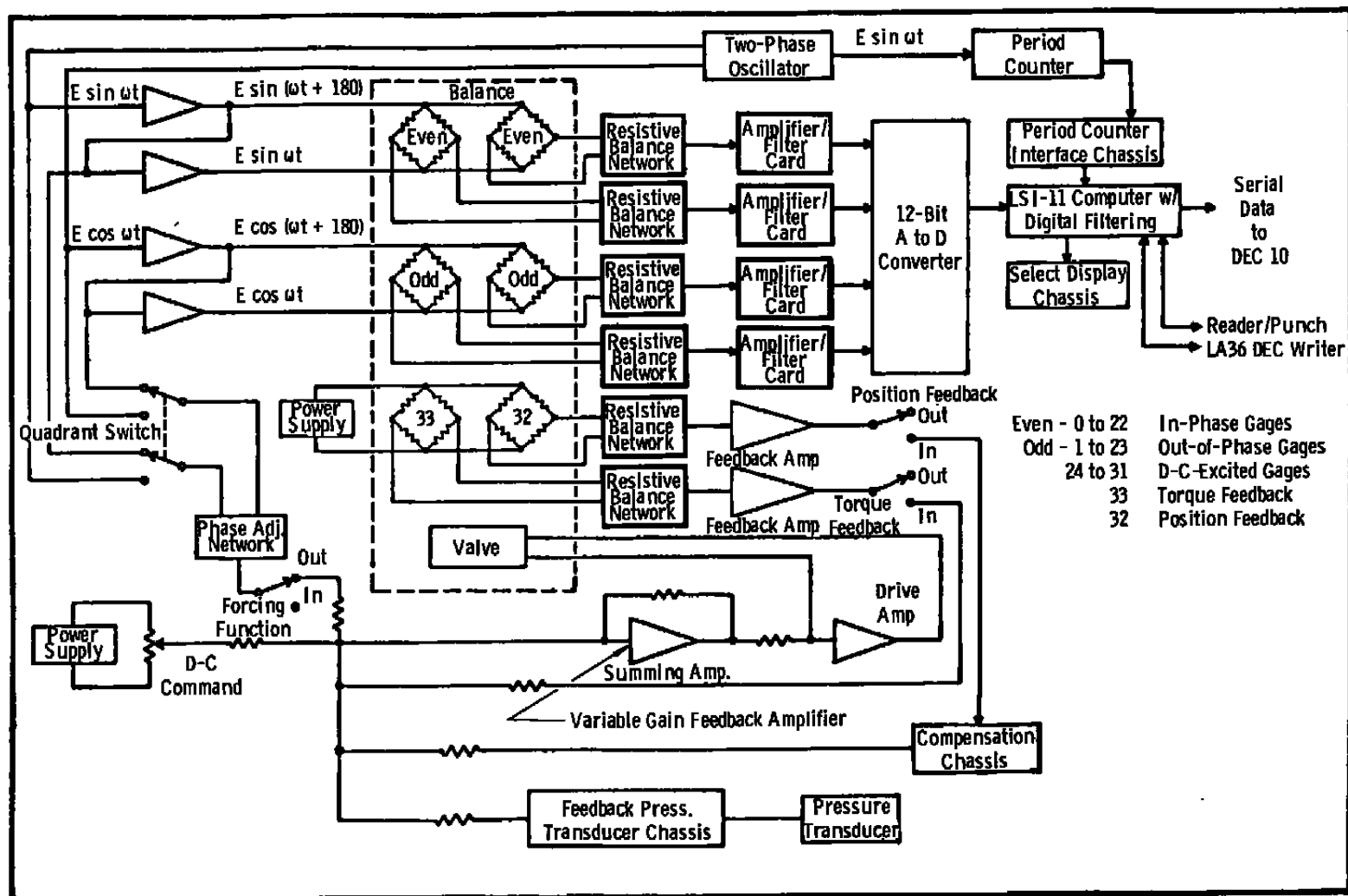


Figure 10. Forced-oscillation balance control and readout system block diagram.

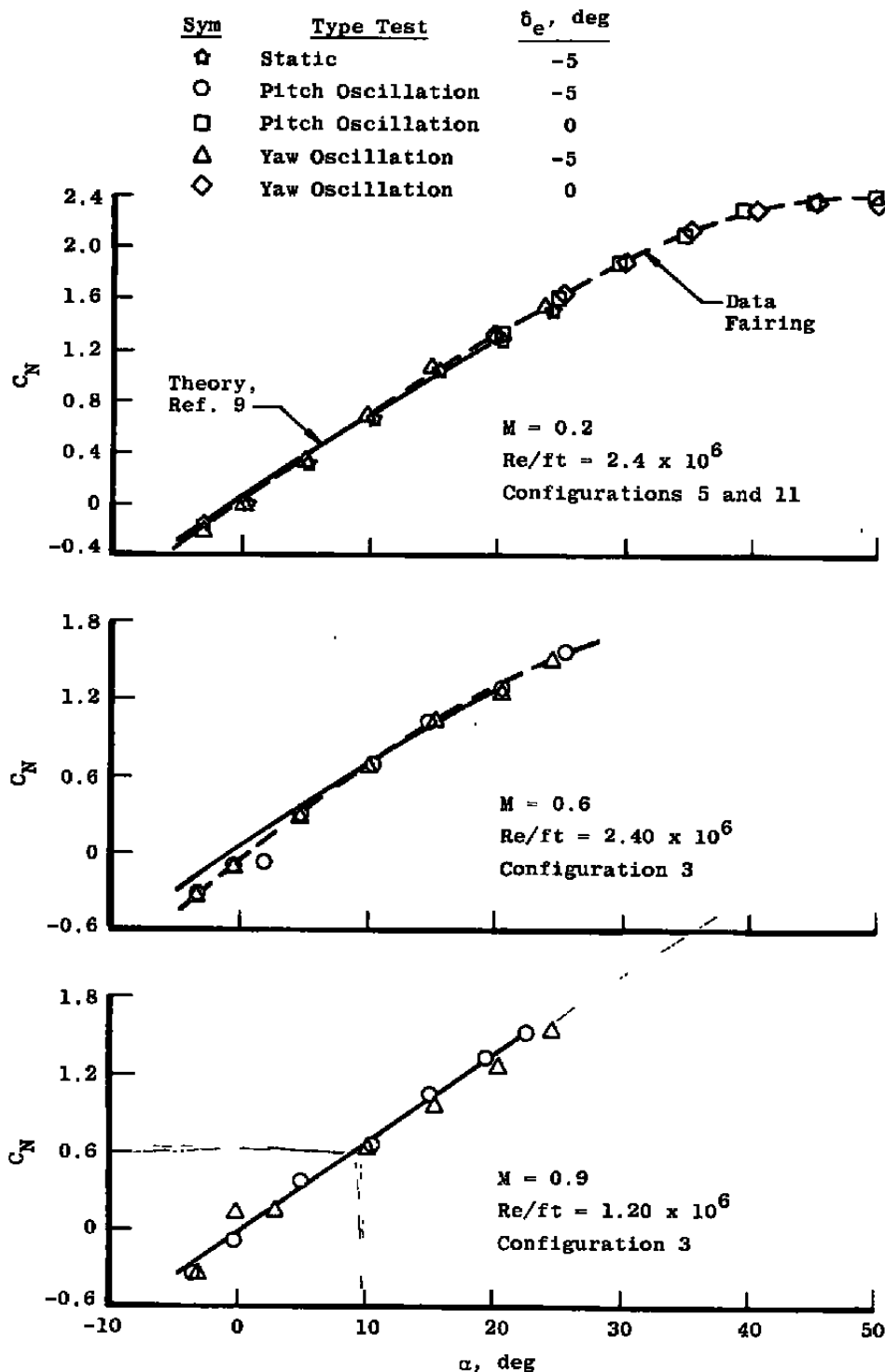
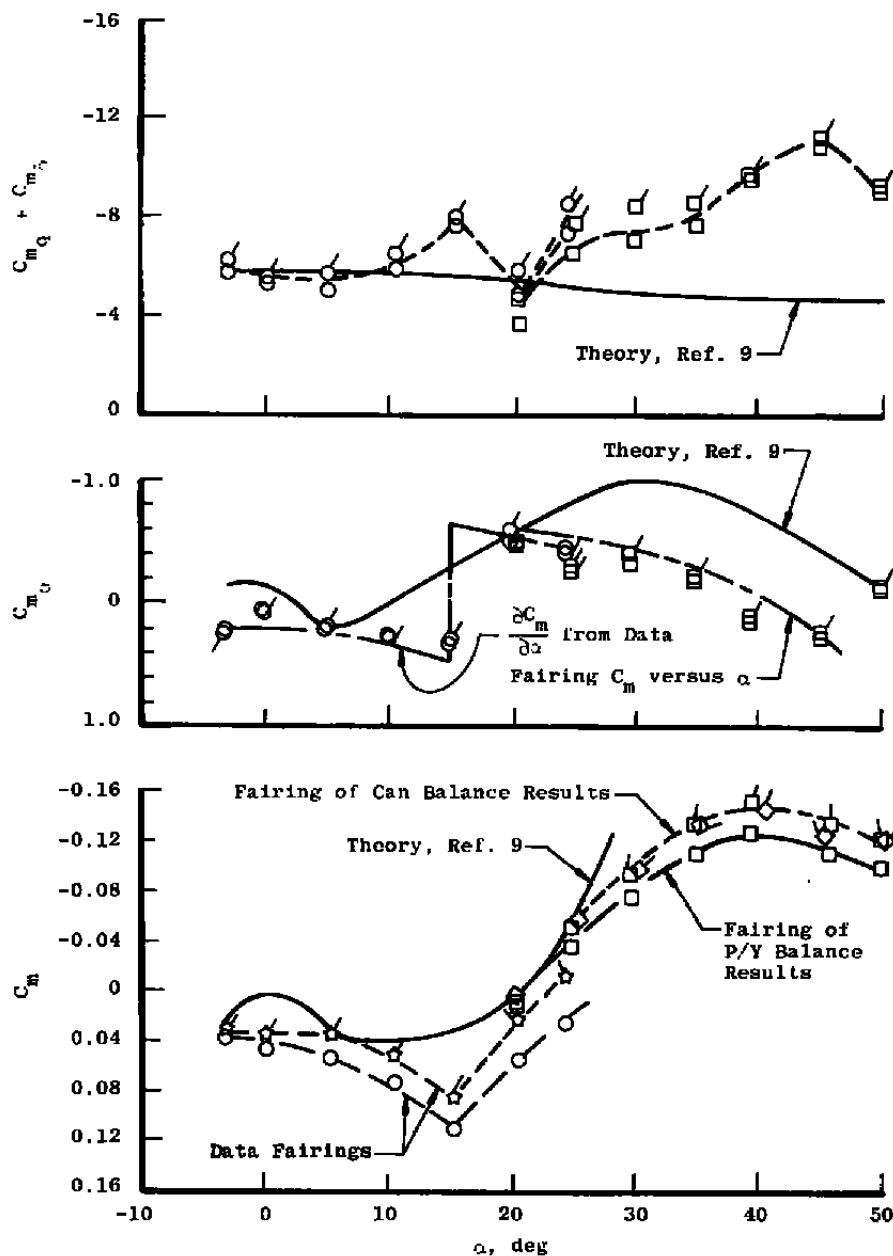


Figure 11. Static normal-force coefficient.

Sym	δ_e , deg	$R_0/ft \times 10^6$	Type Test	Configuration
☆	-5	2.4	Static	5
○	-5	2.4	Pitch Oscillation	5
□	0	1.2	Pitch Oscillation	11
◇	0	1.2	Yaw Oscillation	11

Flagged Symbols Denote Can Balance Results

Plain Symbols Denote P/Y Balance Results



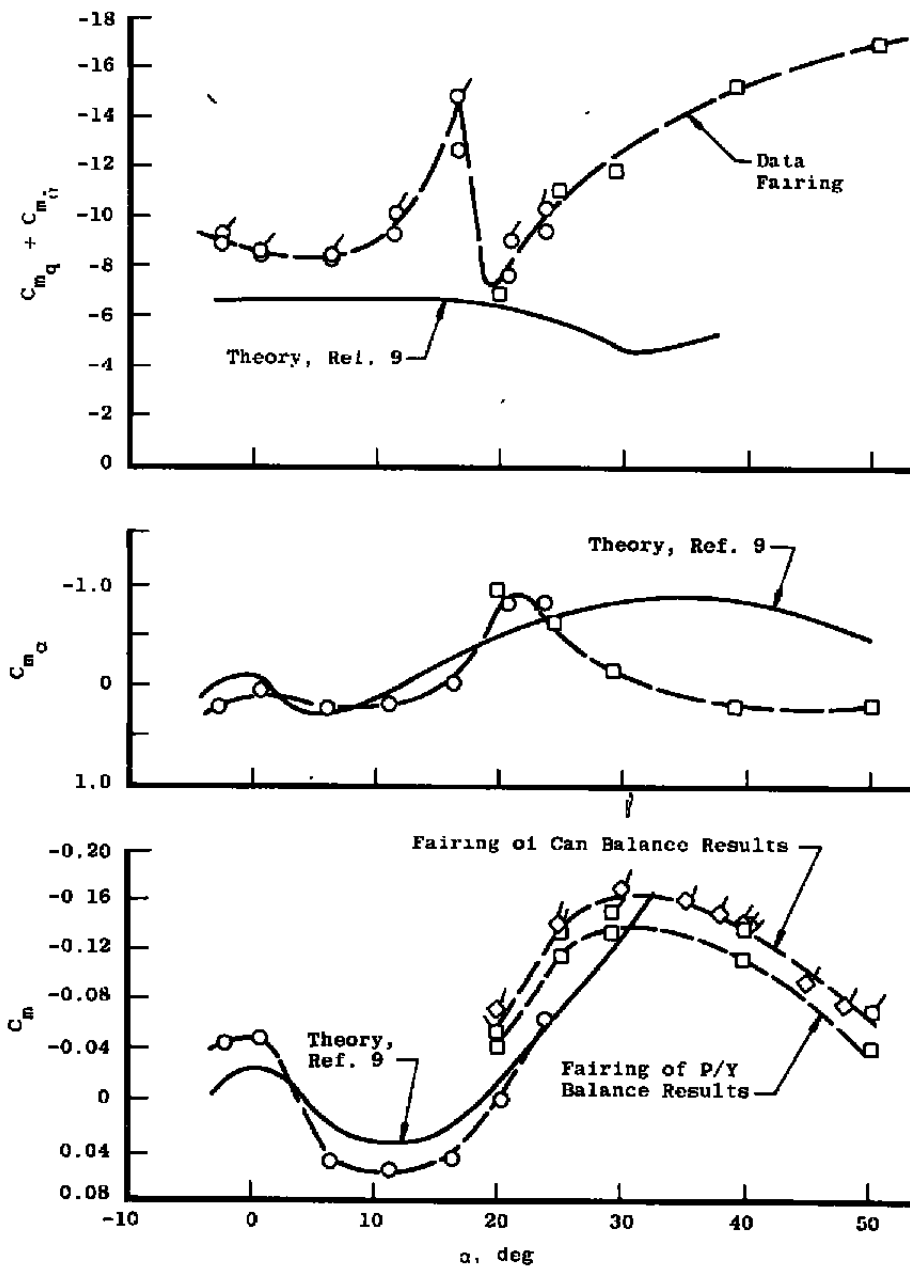
a. $M = 0.2$, $RFP = 0.10$

Figure 12. Longitudinal stability results.

Sym	δ_e , deg	Re/ft $\times 10^6$	Type Test	Configuration
○	-5	2.4	Pitch Oscillation	5
□	0	1.2	Pitch Oscillation	11
◇	0	1.2	Yaw Oscillation	11

Flagged Symbols Denote Can Balance Results

Plain Symbols Denote P/Y Balance Results



b. $M = 0.8$, $RFP = 0.02$

Figure 12. Concluded.

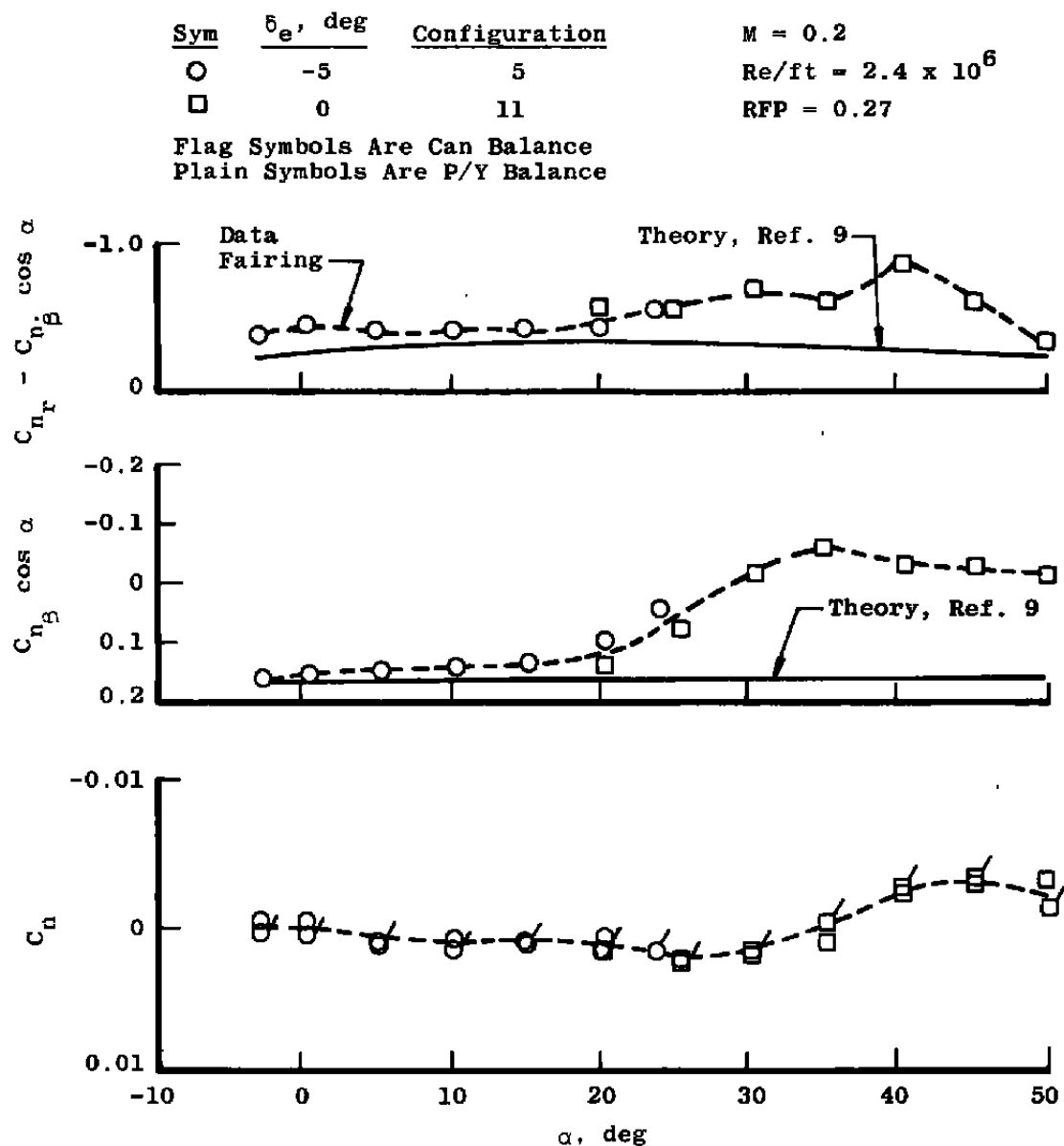


Figure 13. Lateral stability results.

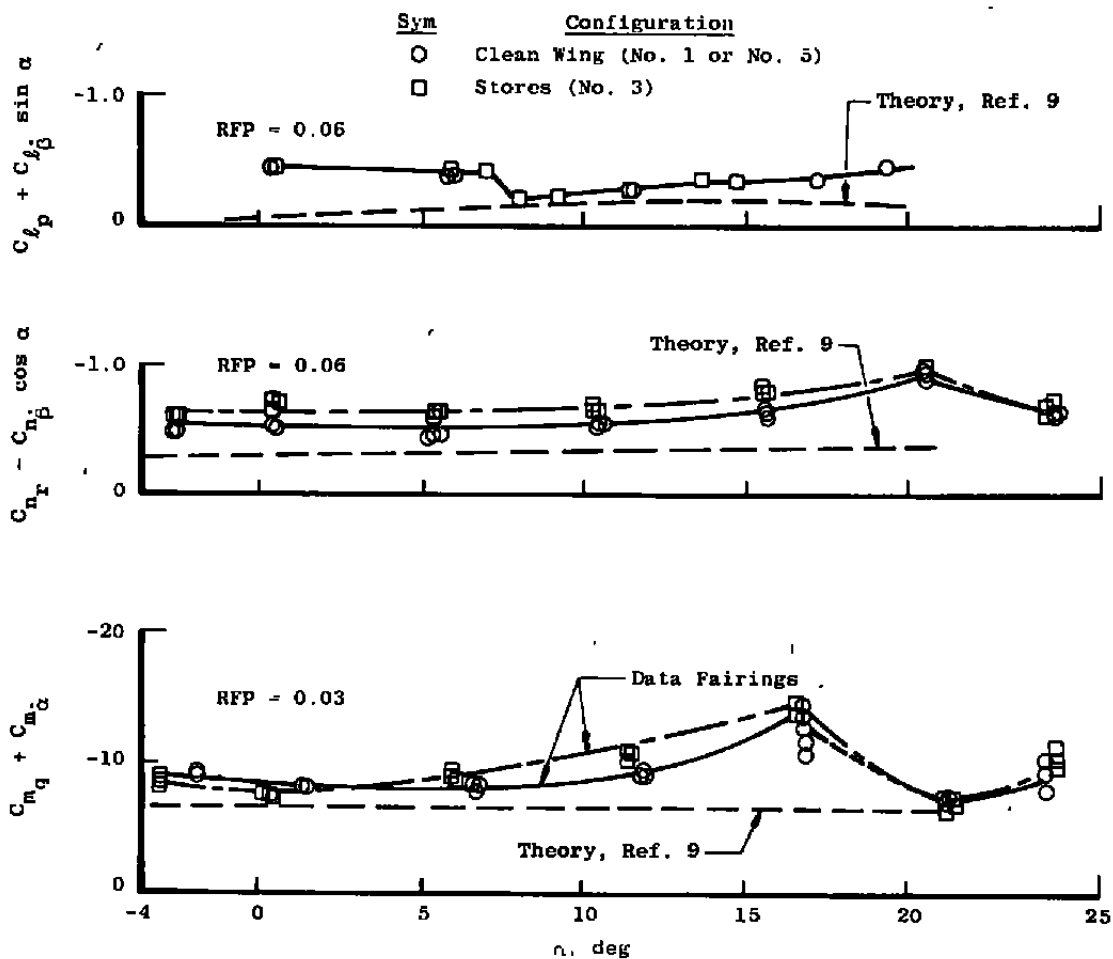


Figure 14. Effects of external stores on the damping derivatives at $M = 0.8$.

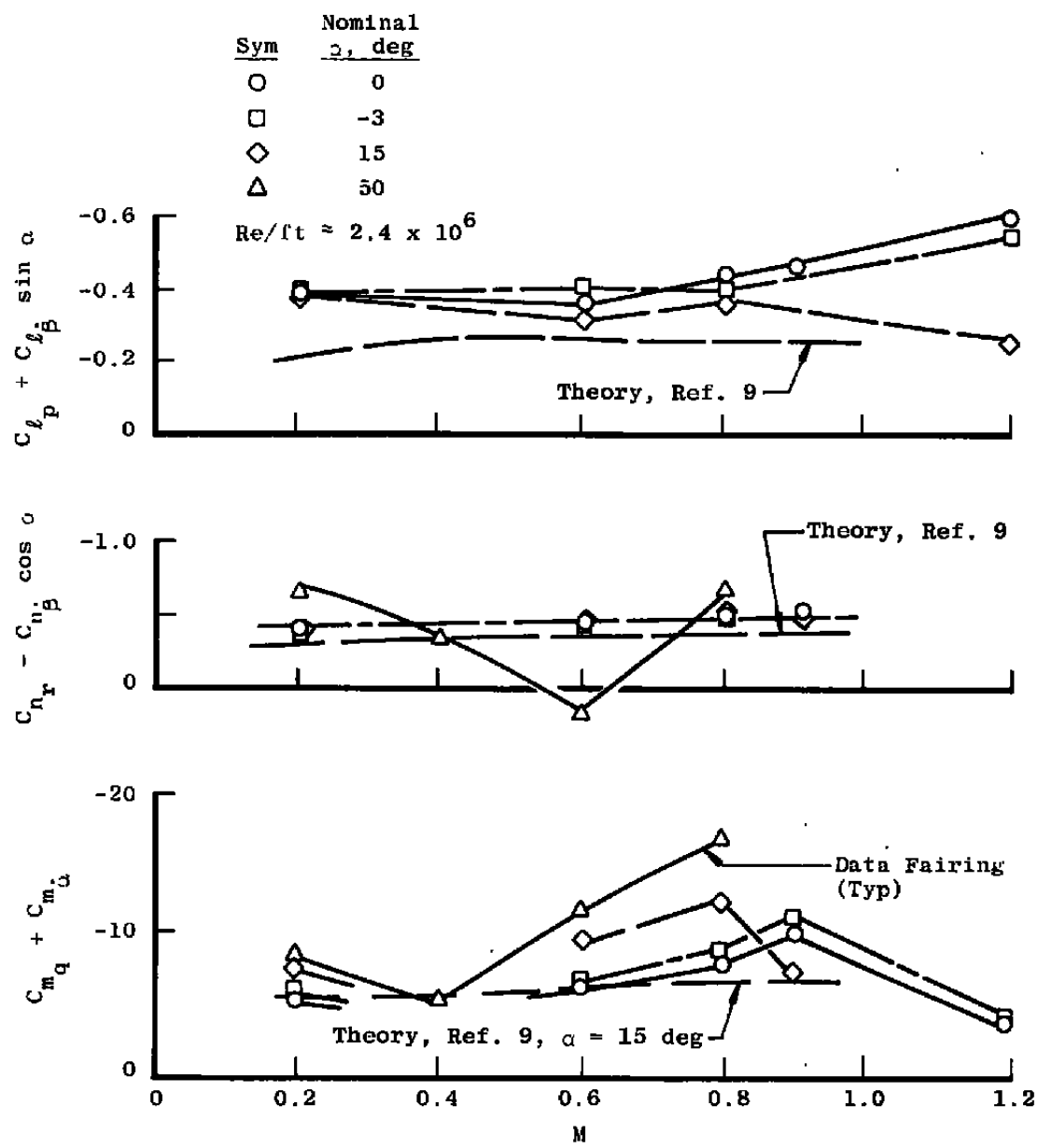


Figure 15. Effect of Mach number on the damping derivatives.

Sym	δ_e , deg	Balance
O	-10	Roll
X	-5	P/Y*
Δ	0	P/Y*

$M = 0.2$

$Re/ft = 2.5 \times 10^6$

Configurations 1, 5, 11

$RFP \approx 0.27$

$$*C_{n_\beta} \sin \alpha = (C_{n_\beta} \cos \alpha) \cdot \tan \alpha$$

where

$C_{n_\beta} \cos \alpha$ is from P/Y Balance.

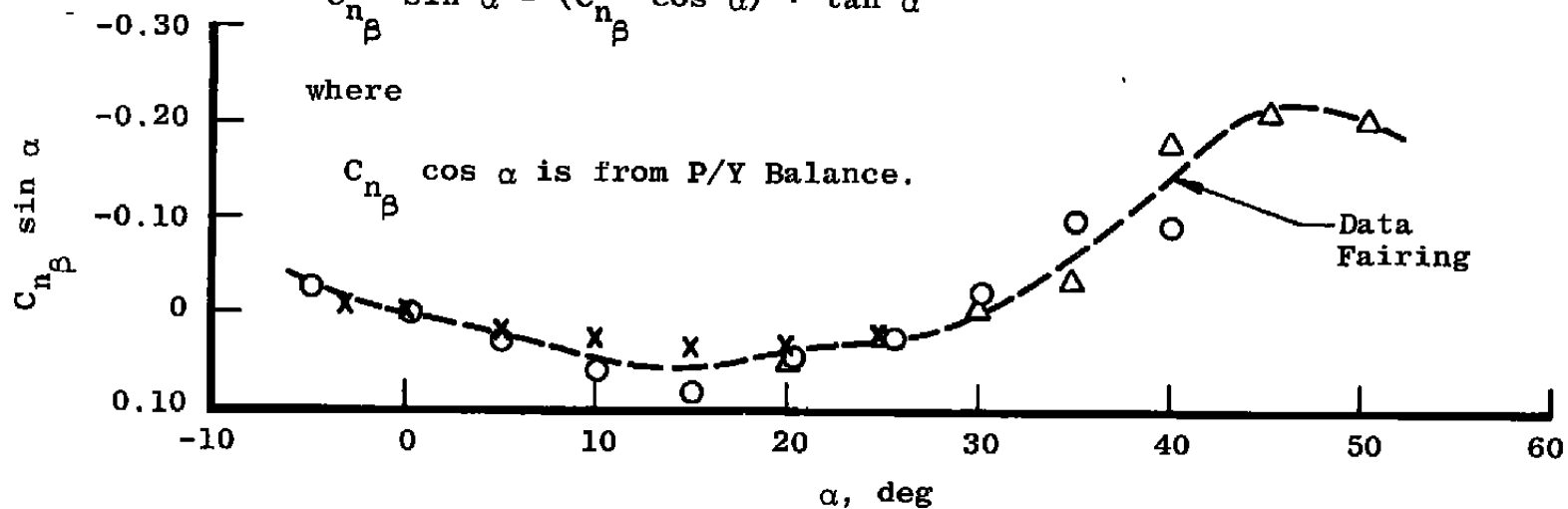
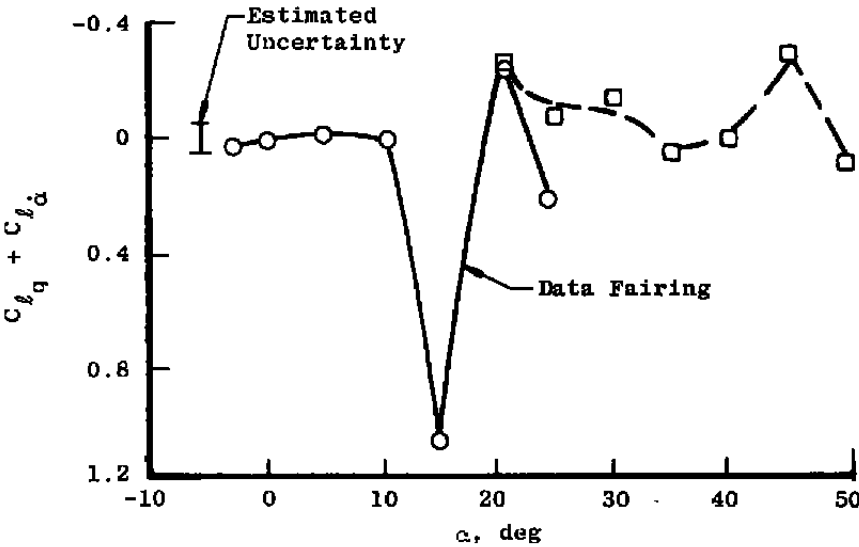
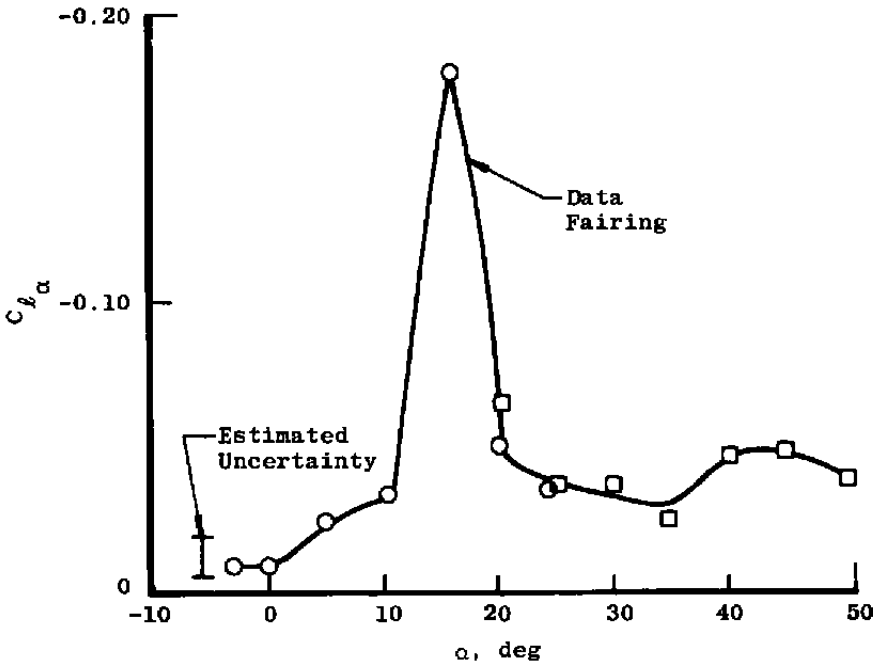


Figure 16. Static yawing-moment derivative, $C_{n_\beta} \sin \alpha$.

Sym	$\bar{\alpha}_e$, deg	Configuration	M = 0.2
○	-5	5	Re/ft = 2.4×10^6
□	0	11	RFP = 0.11

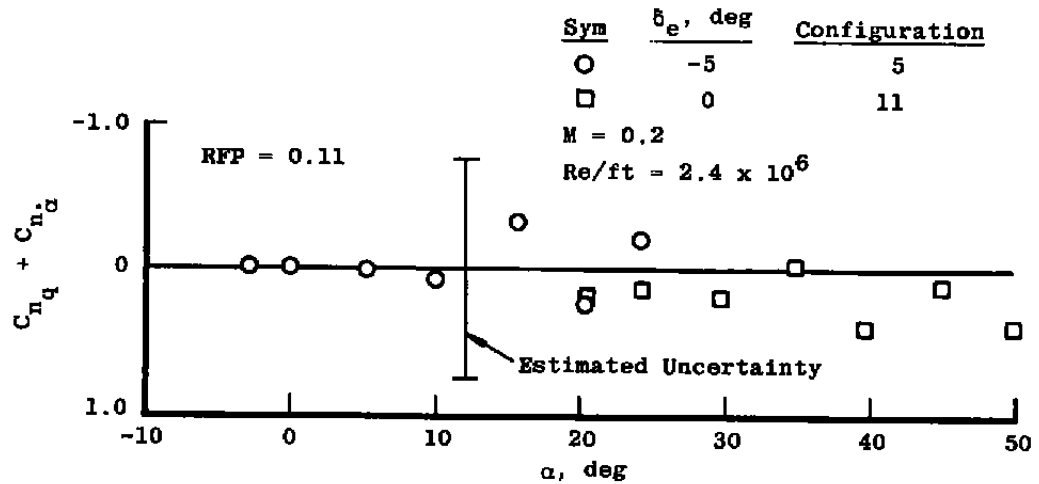


a. Dynamic cross-coupling rolling moment

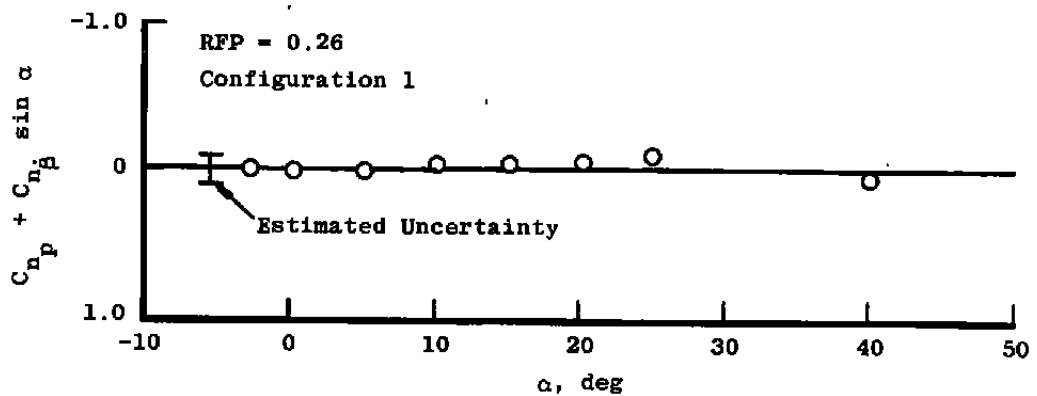


b. Static cross-coupling rolling moment

Figure 17. Cross and cross-coupling derivative results.



c. Dynamic cross-coupling yawing moment



d. Dynamic cross derivative yawing moment

Figure 17. Concluded.

Table 1. Balance Design Capabilities

Balance	Static Derivative	Dynamic Derivatives		
		Direct	Cross	Cross-Coupling
Roll Dynamic ^{a,c}	$C_{n_\beta} \sin \alpha$ $C_{l_\beta} \cos \alpha$	$C_{l_p} + C_{l_\beta} \sin \alpha$	$C_{n_p} + C_{n_\beta} \sin \alpha$	None
P/Y Dynamic ^b Pitch Osc.	C_{m_α}	$C_{m_q} + C_{m_\alpha}$	None	None
Yaw Osc.	$C_{n_\beta} \cos \alpha,$	$C_{n_r} - C_{n_\beta} \cos \alpha$	None	None
Can Balance ^c Pitch Osc.	$C_{m_\alpha}, C_{l_\alpha}$ $C_{N_\alpha}, C_{n_\alpha}$ C_{Y_α}	$C_{m_q} + C_{m_\alpha}$ $C_{N_q} + C_{N_\alpha}$	N/A	$C_{l_q} + C_{l_\alpha}$ $C_{n_q} + C_{n_\alpha}$
Yaw Osc.	$C_{n_\beta} \cos \alpha, C_{l_\beta} \cos \alpha$ $C_{N_\beta} \cos \alpha, C_{m_\beta} \cos \alpha$ $C_{Y_\beta} \cos \alpha$	$C_{n_r} - C_{n_\beta} \cos \alpha$ $C_{Y_r} - C_{n_\beta} \cos \alpha$	$C_{l_r} - C_{l_\beta} \cos \alpha$	$C_{m_r} - C_{m_\beta} \cos \alpha$

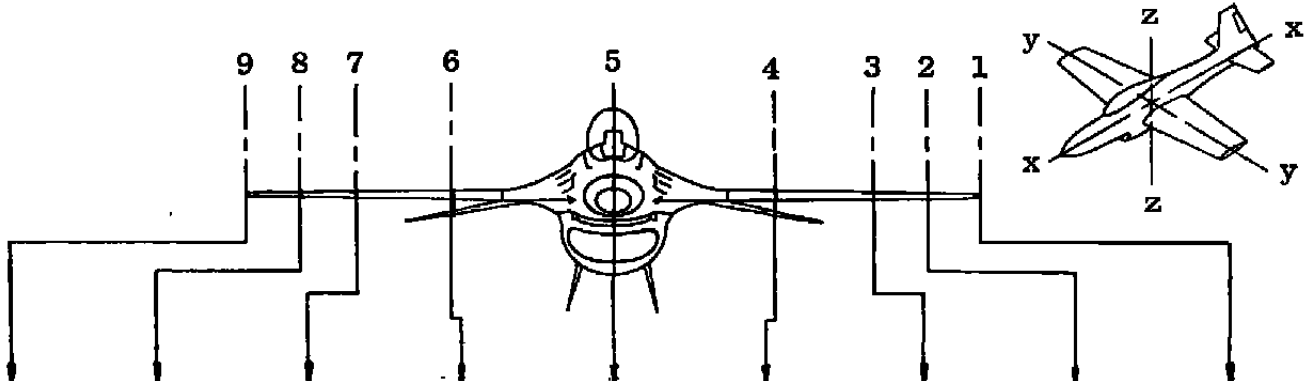
Notes: a. Operational $\alpha < 15$ deg
b. Operational $\alpha < 50$ deg
c. Needs further development

Table 2. Natural Frequency Effects

Balance	Balance Component	Derivative	Natural Frequency, Hz	Estimated ^a Magnification (Bias) Error, Percent
Roll 5-Component Can	Yawing Moment	$C_{n_p} + C_{n_\beta} \sin \alpha$	41	2
	Pitching Moment	$C_{m_q} + C_{m_{\dot{\alpha}}}$ or	115	<1
		$C_{m_r} - C_{m_\beta} \cos \alpha$	115	<1
	Yawing Moment	$C_{n_q} + C_{n_{\dot{\alpha}}}$ or	74	<1
		$C_{n_r} - C_{n_\beta} \cos \alpha$	74	<1
	Rolling Moment	$C_{l_q} + C_{l_{\dot{\alpha}}}$ or	21	9
		$C_{l_r} - C_{l_\beta} \cos \alpha$	21	9

^aCalculated for an oscillation frequency of 6 Hz.

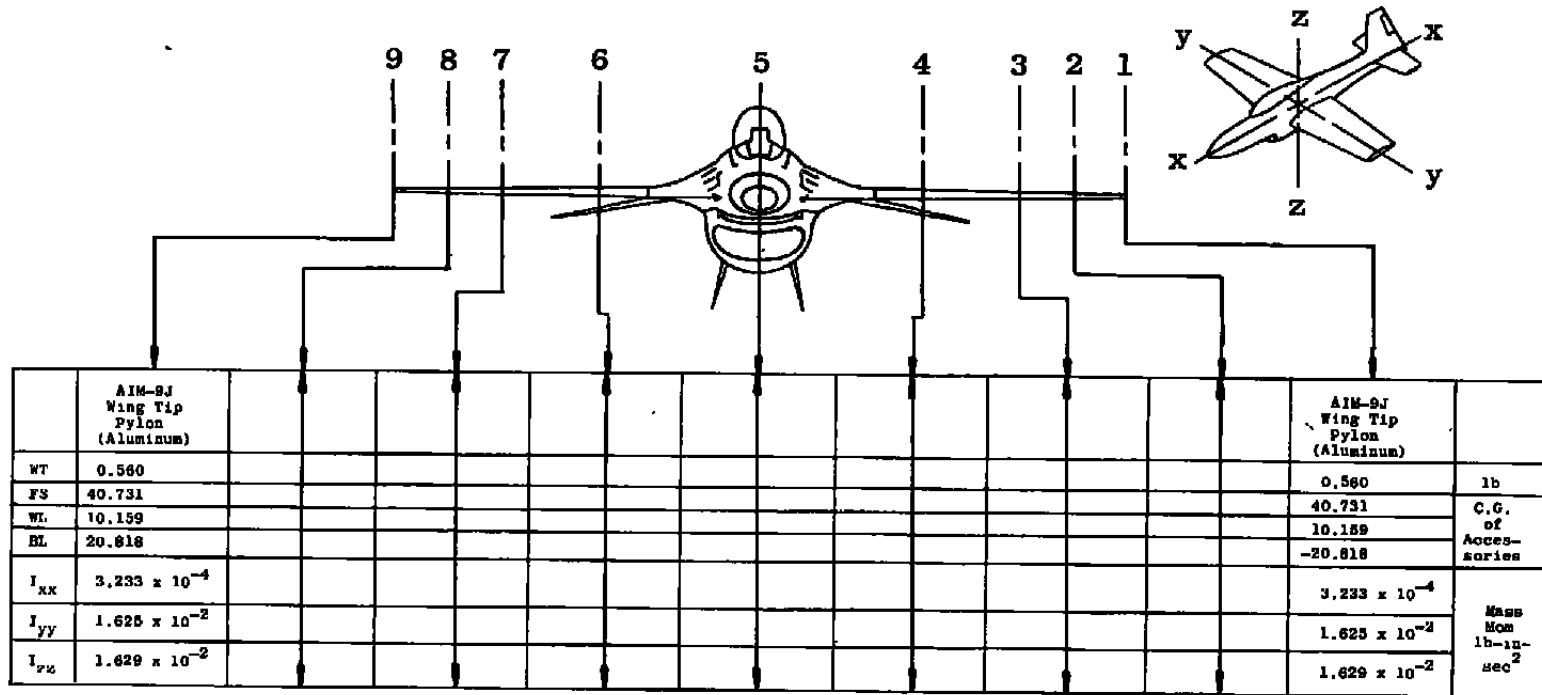
Table 3. Aircraft Stores Details, Configuration 3



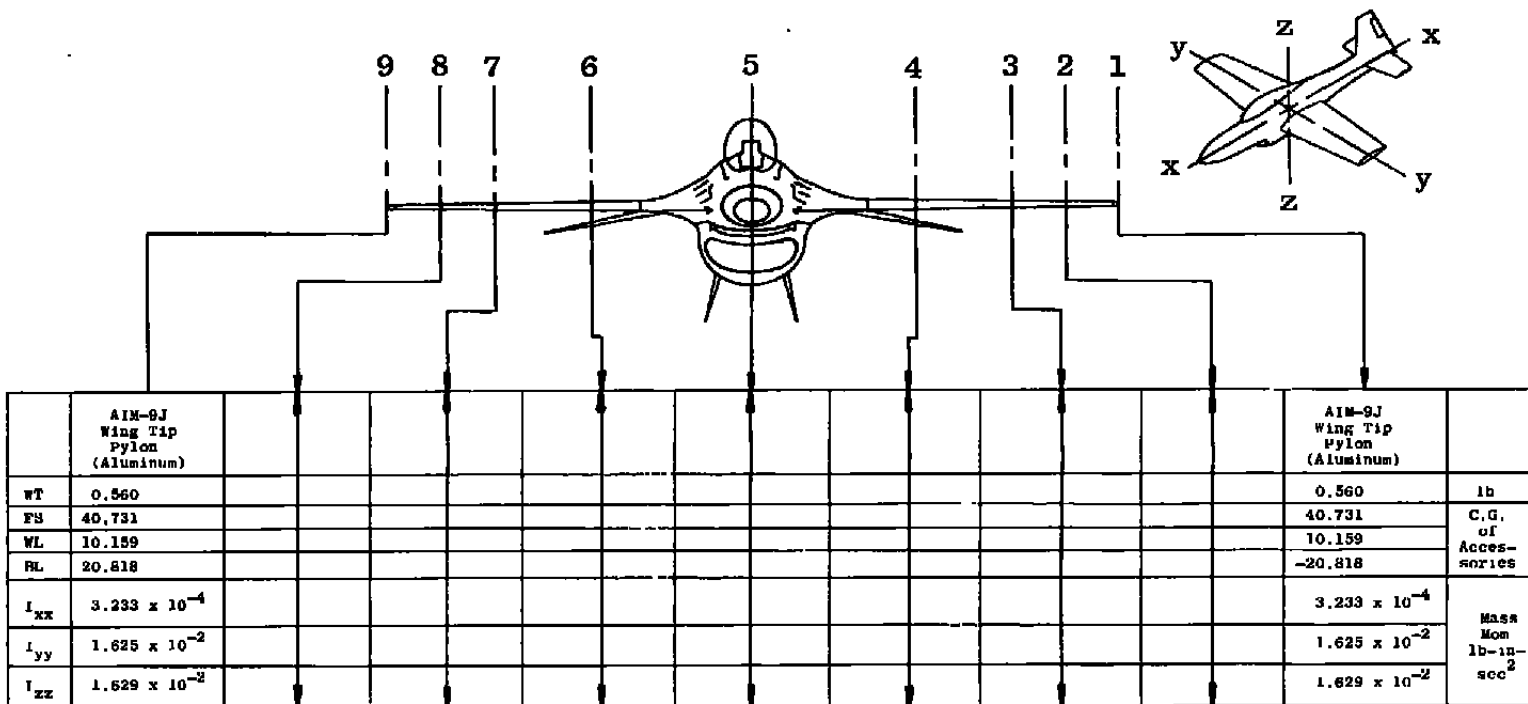
	AIM-9J Wing Tip Pylon (Aluminum)		3 AGM-65 Triple Rail Launcher Weapons Pylon	370-Gal Fuel Tank & Pylon	ALQ-119-12 ECM & Pylon	370-Gal Fuel Tank & Pylon	3 AGM-65 Triple Rail Launcher Weapons Pylon		AIM-9J Wing Tip Pylon (Aluminum)	
WT	0.560		6.439	5.564	1.691	5.564	6.439		0.560	lb
FS	40.731		38.476	33.652	35.157	33.652	38.476		40.731	C. G. of Aircraft Stores
WL	10.159		7.926	7.200	5.000	7.200	7.926		10.159	
BL	20.818		13.333	7.889	-0.001	-7.889	-13.333		-20.818	
I_{xx}	3.233×10^{-4}		3.764×10^{-2}	2.841×10^{-2}	2.467×10^{-3}	2.841×10^{-2}	3.764×10^{-2}		3.233×10^{-4}	Mass Mom lb-in- sec ²
I_{yy}	1.625×10^{-2}		1.143×10^{-1}	4.806×10^{-1}	9.655×10^{-2}	4.806×10^{-1}	1.143×10^{-1}		1.625×10^{-2}	
I_{zz}	1.629×10^{-2}		1.285×10^{-1}	4.712×10^{-1}	9.502×10^{-2}	4.712×10^{-1}	1.285×10^{-1}		1.629×10^{-2}	

1/9 F16 Aircraft & Stores Combination		
Weight (lb)	C.G. Location	Mass Mom Inertia (lb-in-sec ²)
150,307	FS 36.0780	$I_{xx} = 17.05$
	WL 9.6331	$I_{yy} = 59.43$
	BL -0.0000	$I_{zz} = 71.96$

52



1/9 F16 Aircraft & Stores Combination		
Weight (lb)	C.G. Location	Mass Mom Inertia (lb-in-sec ²)
124.610	F5 36.0594	I _{xx} = 13.8
	WL 10.0896	I _{yy} = 44.78
	BL 0.0000	I _{zz} = 52.31

Table 5. Aircraft Stores Details, Configuration 11

1/8 F16 Aircraft & Stores Combination		
Weight (lb)	C.G. Location	Mass Mom Inertia (lb-in-sec ²)
124,030	FX 36.1517	I _{xx} = 7.89
	W1. 10.0995	I _{yy} = 44.78
	BL 0.0000	I _{zz} = 51.39

Table 6. Configuration Chart

Config No.	Inlet Fairing	δ LE' Deg	δ e' Deg	Right Wing-Tip	Right-Wing Pylon Station			Fuselage	Left-Wing Pylon Station			Left Wing-Tip		
					Store Locations									
					9	8	7		6	5	4		3	2
1	yes	0	-10	AIM-9J ¹	-	-	-	-	-	-	-	AIM-9J ^b		
3	yes	↓	0 ^a	AIM-9J	-	AGM-65 (3)	370-gal Tank	ECM ALQ-119V	370-gal Tank	AGM-65 (3)	-	AIM-9J		
4	yes		-10	AIM-9J ^b	-	-	370-gal Tank	300-gal Tank	370-gal Tank	-	-	AIM-9J ^b		
5	yes		-5	AIM-9J	-	-	-	-	-	-	-	AIM-9J		
9	no		-10	AIM-9J ^b	-	-	-	-	-	-	-	AIM-9J ^b		
11	no		0 ^a	AIM-9J	-	-	-	-	-	-	-	AIM-9J		
12	no	25	0	↓	-	-	-	-	-	-	-	↓		
13 Nose Strake	no	25	0	↓	-	-	-	-	-	-	-	↓		
20	no	0	-10	-	-	-	-	-	-	-	-	-		
21	no	0	0	AIM-9J Launcher Only	-	-	-	-	-	-	-	AIM-9J Launcher Only		
22	no	25	0	↓	-	-	-	-	-	-	-	↓		
23 Nose Strake	no	25	0	↓	-	-	-	-	-	-	-	↓		

^a δ_Q = -10 deg for roll test phase.

^b Special high inertia AIM-9J missile.

Table 7. Typical Installation Natural Frequencies

Component	Natural Frequencies, Hz	
	Pitch Plane	Yaw Plane
Model Sting	11.5	11.5
Guy Rods	25	46
Wings (Spanwise)	50	-
Test Section Sector	65	34.5
Wings (Chordwise)	132	-

Table 8. Test Summary

Config	Type of Data	M	Re/ft $\times 10^{-6}$	α Range, deg
1 ↓	Roll ↓	0.2	2.4	-5 to 40
		0.6	1.2	0 to 10
		0.6	2.4	-5 to 27
		0.8	↓	-5 to 19
		0.9	↓	0 to 11
		1.2	↓	0 to 34
		1.4	↓	0 to 22
3 ↓	Roll ↓	0.2	2.4	-5 to 20
		0.6	↓	-5 to 15
		0.8	↓	-6 to 14
		0.9	↓	-5 to 13
	Pitch ↓	0.2	2.4	-3 to 24
		0.6	↓	-3 to 14
		0.8	↓	-3 to 24
		0.9	↓	-3 to 20
	Yaw ↓	0.2	2.4	-3 to 24
		0.6	2.4	↓
		0.8	1.2	↓
		0.9	1.2	↓
		0.9	2.4	-3 to 10
4 ↓	Roll ↓	0.2	2.4	-5
		0.6	↓	-5 to 13
		0.8	↓	-5 to 11
		0.9	↓	0 to 11
		1.2	↓	-5 to 22
5 ↓	Pitch ↓	0.2	2.4	-3 to 24
		0.6	↓	-3 to 15
		0.8	↓	-3 to 24
		0.9	↓	-3 to 21
		1.2	1.2	-3 to 10
	Yaw ↓	0.2	2.4	-3 to 24
		0.6	2.4	-3 to 15
		0.8	1.2	-3 to 24
		0.9	1.2	0 to 20

Table 8. Concluded

Config	Type of Data	M	Re/ft x 10 ⁻⁶	α Range, deg
9	Roll	0.6	2.4	0 to 16
11	Roll	0.2	2.4	0 to 36
↓	↓	0.6	↓	0 to 11
↓	↓	0.8	↓	0 to 11
↓	Pitch	0.2	2.4	20 to 50
↓	↓	0.4	2.4	20 to 50
↓	↓	0.6	1.2	20 to 50
↓	↓	0.6	2.4	20, 25
↓	↓	0.8	1.2	20 to 50
↓	Yaw	0.2	2.4	20 to 50
↓	↓	0.4	2.4	↓
↓	↓	0.6	1.2	↓
↓	↓	0.8	1.2	↓
12	Yaw	0.2	1.2	20 to 50
↓	↓	0.2	2.4	20 to 50
↓	↓	0.4	2.4	20 to 45
↓	↓	0.6	1.2	20 to 50
13	Yaw	0.2	2.4	20 to 50
13	Yaw	0.4	2.4	20 to 47.5
20	Roll	0.6	2.4	0 to 11
20	Roll	0.8	2.4	0 to 11
21	Pitch	0.2	2.4	20 to 50
21	Pitch	0.8	1.2	20 to 50
22	Pitch	0.2	1.2	20, 50
↓	↓	0.2	2.4	20 to 50
↓	↓	0.4	2.4	20 to 50
↓	↓	0.6	1.2	20 to 50
23	Pitch	0.2	2.4	20 to 50
23	Pitch	0.4	2.4	20 to 50

Table 9. Uncertainties

Parameter Designation	STEADY-STATE ESTIMATED MEASUREMENT*							Range	Type of Measuring Device	Type of Recording Device	Method of System Calibration
	Precision Index (S)			Bias (B)		Uncertainty $\pm(B + 1.95S)$					
	Percent of Reading	Unit of Measurement	Degree of Freedom	Percent of Reading	Unit of Measurement	Percent of Reading	Unit of Measurement				
Tunnel Stilling Chamber pressure (P_t), psf		0.45 0.40	33		1.70 1.40		2.60 2.20	1900 1300	Datametrics ↓	DDAS ↓	In-Place Dead weight tester ↓
Tunnel Plenum Chamber Pressure (P_c), psf		0.45 0.37	33		1.70 1.30		2.60 2.04	1900 860			
Tunnel Stilling Chamber Temperature, (T_t), °F		0.70 0.70	8		2.50 2.50		4.11 4.11	94 110	Digital Fluke Meter		None
Model Sector Pitch Angle (α), deg		0.10	25		0		0.10	all	Potentiometer		Inclinometer Comparison-In-Place
Model Oscillation Rate (ω), rad/sec		0.003	2		0		0.01	30-50	Frequency Counter	Forced Oscillation Balance Control and Recording System (FOBCARS) ↓	Frequency Substitution
Static Normal Force (F_N), lb	0.3	0.5	20		0 0	0.6	1	0-200 >200	Bonded Strain Gages on Can Balance ↓		Static Loading ↓
Static Pitching Moment (M_m), ft-lb	0.3	0.5	20		0	0.6	1	<250 >250			

Table 9. Continued
a. Concluded

Parameter Designation	STEADY-STATE ESTIMATED MEASUREMENT*							Range	Type of Measuring Device	Type of Recording Device	Method of System Calibration
	Precision Index (S)			Bias (B)		Uncertainty $\pm(B + t_{95}S)$					
	Percent of Reading	Unit of Measurement	Degree of Freedom	Percent of Reading	Unit of Measurement	Percent of Reading	Unit of Measurement				
Static Side Force (F_L), lb	0.3	0.05	20	0		0.6	0.1	+25 -25	Can Balance ↓	FOBCARS ↓	Static Loading ↓
Static Yawing Moment (M_n), ft-lb	0.3	0.10	20	0		0.6	0.2	+50 -50			
Static Rolling Moment (M_r), ft-lb	0.3	0.02	20	0		0.6	0.04	+10 -10			
Static Sting Moment (MS2), ft-lb		4.0	20	0			8.0	All			

Table 9. Continued
b. Basic Dynamic Measurements

Parameter Designation	STEADY-STATE ESTIMATED MEASUREMENT*							Range	Type of Measuring Device	Type of Recording Device	Method of System Calibration
	Precision Index (S)			Bias (B)		Uncertainty $\pm(B + t95S)$					
	Percent of Reading	Unit of Measurement	Degree of Freedom	Percent of Reading	Unit of Measurement	Percent of Reading	Unit of Measurement				
Model Oscillation Amplitude (θ), deg		0.02	20		0		0.04	± 2	Bonded Strain Gage on Forced Oscillation Balance ↓	FOBCARS ↓	Static Loading
In-Phase Torque (TORI), ft-lb	0.5	0.02	20		0 0		1.0 0.04	< 4 > 4			Static and Dynamic Loading ↓
Out-of-Phase Torque (TORQ), ft-lb	0.5	0.02	20		0 0		1.0 0.04	< 4 > 4			
In-Phase Stang Moment (MS21), ft-lb		4.0	20		0		8.0	All	Bonded Strain Gage on Stang ↓		Static Loading ↓
Out-of-Phase Stang Moment (MS24), ft-lb		4.0	20		0		8.0	All			
In-Phase Pitching Moment (M_{PI}), ft-lb	0.3	0.5	20		0		0.6 1	< 250 > 250	Can Balance ↓	FOBCARS ↓	Static and Dynamic Loading ↓
Out-of-Phase Pitching Moment (M_{PO}), ft-lb	0.3	0.5	20		0		0.6 1	< 250 > 250			
In-Phase Yawing Moment (M_{YI}), ft-lb	0.3	0.10	20		0		0.6 0.2	< 50 > 50			

Table 9. Continued
b. Concluded

Parameter Designation	STEADY-STATE ESTIMATED MEASUREMENT*							Range	Type of Measuring Device	Type of Recording Device	Method of System Calibration
	Precision Index (S)			Bias (B)		Uncertainty $\pm(B + 1.96S)$					
	Percent of Reading	Unit of Measurement	Degree of Freedom	Percent of Reading	Unit of Measurement	Percent of Reading	Unit of Measurement				
Out-of-Phase Yawing Moment (M_{nQ}), ft-lb	0.3	0.10	20		0	0.6	0.2	-50 +50	Can Balance ↓	FORCARS ↓	Static and Dynamic Loading ↓
In-Phase Rolling Moment (M_{rI}), ft-lb	0.3	0.02	20		0		0.04	-10 +10			
Out-of-Phase Rolling Moment (M_{rQ}), ft-lb	0.3	0.02	20		0	0.6	0.04	-10 +10			

Table 9. Continued
c. Calculated Parameters

Parameter Designation	STEADY-STATE ESTIMATED MEASUREMENT*							Range
	Precision Index (S)			Bias (B)		Uncertainty $\pm(B + t_{95}S)^a$		
	Percent of Reading	Unit of Measurement	Degree of Freedom	Percent of Reading	Unit of Measurement	Percent of Reading	Unit of Measurement	
M		0.002 0.0005			0.002 0.002		0.006 0.003	0.2 0.8
P, psf		1.1 0.4			1.7 1.3		3.9 2.1	3800 860
q, psf		1.6 0.4			2.3 1.3		5.5 2.1	106 387
Re/ft x 10 ⁻⁶		0.02 0.002			0.03 0.005		0.07 0.009	2.4 2.4
V, ft/sec		2.3 1.0			2.5 3.5		7.1 5.5	230 880
RFP	1 0.1			1 0.4		3 0.6		All at M = 0.2 All at M = 0.8

^a $t_{95} = 2$ for all calculated parameters.

Table 9. Continued
c. Continued

Parameter Designation	STEADY-STATE ESTIMATED MEASUREMENT*							Range	Test Condition			Balance
	Precision Index (S)			Bias (B)		Uncertainty $\pm(B + t_{95}S)$			M	Re/ft $\times 10^{-6}$	s	
	Percent of Reading	Unit of Measurement	Degree of Freedom	Percent of Reading	Unit of Measurement	Percent of Reading	Unit of Measurement					
C_m	0.001 0.003 0.0003 0.0003			0 0.001 0.0002 0		0.002 0.007 0.0008 0.0006	0.050 0.057 0.044 -0.064	0.2 0.2 0.8 0.8	2.4	0.2 20 0.8 24	P/Y Balance	
C_{m_α}	0.010 0.012 0.003 0.003			0.012 0.011 0.006 0.012		0.032 0.035 0.012 0.018	0.051 0.600 0.073 -0.840	0.2 0.2 0.8 0.8		0.2 20 0.8 24		
$C_{m_q} + C_{m_{\dot{\alpha}}}$	0.10 0.09 0.16 0.13			0.06 0.07 0.03 0.03		0.26 0.25 0.35 0.29	-5.31 -4.87 -8.32 -9.43	0.2 0.2 0.8 0.8		0.2 20 0.8 24		
C_n	0.0004 0.0010 0.0001 0.0001			0 0 0 0		0.0008 0.0024 0.0002 0.0002	-2.6×10^{-4} -1.9×10^{-3} 7.7×10^{-4} 4.0×10^{-4}	0.2 0.2 0.8 0.8	1.2	0.0 20 0.0 20		
$C_{n_\beta} \cos \phi$	0.003 0.003 0.002 0.002			0.003 0.002 0.003 0.001		0.009 0.008 0.007 0.005	0.146 0.043 0.175 0.031	0.2 0.2 0.8 0.8	2.4 2.4 1.2 1.2	0.0 24 0.0 20		
$C_{n_r} - C_{n_\beta} \cos \phi$	0.010 0.011 0.013 0.017			0.005 0.006 0.001 0.002		0.025 0.028 0.027 0.036	-0.430 -0.520 -0.510 -0.790	0.2 0.2 0.8 0.8	2.4 2.4 1.2 1.2	0 24 0 20		

Table 9. Continued
c. Continued

Parameter Designation	STEADY-STATE ESTIMATED MEASUREMENT*							Range	Test Condition			Balance
	Precision Index (S)			Bias (B)		Uncertainty $\pm(B + t_{95}S)$						
	Percent of Reading	Unit of Measurement	Degree of Freedom	Percent of Reading	Unit of Measurement	Percent of Reading	Unit of Measurement		M	Re/ $t_1 \times 10^{-6}$	n	
C_N		0.003 0.008 0.001 0.009			0.0004 0.0030 0.0004 0.0089		0.006 0.0019 0.0024 0.027	0.017 0.157 0.070 1.640	0.2 0.2 0.8 0.8	2.4	0.2 20 0.8 24	Can Balance <

Table 9. Continued
c. Continued

Parameter Designation	STEADY-STATE ESTIMATED MEASUREMENT*							Range	Test Condition			Balance
	Precision Index (S)			Bias (B)		Uncertainty $\pm(R + t_{95}S)$						
	Percent of Reading	Unit of Measurement	Degree of Freedom	Percent of Reading	Unit of Measurement	Percent of Reading	Unit of Measurement		W	Re/ft $\times 10^{-6}$	"	
C_{m_a}	0.09 0.09 0.03 0.03			0.01 0.01 0.01 0.01		0.19 0.19 0.07 0.07	0.051 0.600 0.073 -0.840	0.2 0.2 0.8 0.8	2.4	0.2 20 0.8 24	Cm Balance	
$C_{m_q} + C_{m_{\dot{\alpha}}}$	1.17 1.13 1.23 1.03			0.06 0.07 0.03 0.03		2.40 2.33 2.49 2.09	-5.31 -4.87 -4.32 -9.43	0.2 0.2 0.8 0.8		0.2 20 0.8 24		
C_{n_a}	0.042 0.042 0.010 0.012			0 0 0 0		0.084 0.084 0.020 0.024	-0.005 -0.006 0.0004 -0.0004	0.2 0.2 0.8 0.8		0.2 20 0.8 24		
$C_{n_q} + C_{n_{\dot{\alpha}}}$	0.39 0.38 0.55 0.37			0 0.02 0 0		0.78 0.78 1.10 0.74	0.01 0.29 -0.18 0.19	0.2 0.2 0.8 0.8		0.2 20 0.8 24		
C_{f_a}	0.001 0.004 0.0004 0.0004			0 0 0 0		0.002 0.008 0.0008 0.0008	-0.005 0.050 0.004 0.008	0.2 0.2 0.8 0.8		0.2 20 0.8 24		
$C_{f_q} + C_{f_{\dot{\alpha}}}$	0.012 0.021 0.014 0.016			0 0.011 0 0.001		0.024 0.053 0.028 0.033	0.013 0.221 -0.058 -0.25	0.2 0.2 0.8 0.8		0.2 20 0.8 24		

Table 9. Concluded
c. Concluded.

Parameter Designation	STEADY-STATE ESTIMATED MEASUREMENT*							Range	Test Condition			Balance
	Precision Index (S)			Bims (B)		Uncertainty $\pm(B + t95S)$						
	Percent of Reading	Unit of Measurement	Degree of Freedom	Percent of Reading	Unit of Measurement	Percent of Reading	Unit of Measurement		M	Rc/ft. $\times 10^{-6}$	s	
C_f	0.0001 0.0001 0.00003 0.00003			0 0 0 0		0.0002 0.0002 0.00006 0.00006	0.0002 0 -0.0002 -0.0001	0.2 0.2 0.8 0.8	2.4	5 35 11 19	Roll Balance	
$C_{fp} + C_{f\beta} \sin \alpha$	0.010 0.008 0.008 0.012			0.020 0.018 0.002 0.003		0.040 0.035 0.018 0.027	-0.43 -0.33 -0.29 -0.48	0.2 0.2 0.8 0.8		5 35 11 19		
$C_{n\beta} \sin \alpha$	0.020 0.020 0.005 0.005			0 0 0 0		0.040 0.040 0.010 0.010	0.000 0.045 0.014 0.050	0.2 0.2 0.8 0.8		0 20 0 19		
$C_{np} + C_{n\beta} \sin \alpha$	0.045 0.050 0.030 0.030			0 0 0 0		0.010 0.100 0.06 0.06	0.040 -0.070 0.063 0.015	0.2 0.2 0.8 0.8		0.8 24 0.8 19		

NOMENCLATURE

B	Bias error, the difference between the average of all measured values and the true value
b	Reference wing span of model, 3.333 ft
BL	Buttock Line, in.
\bar{c}	Reference chord length of model, 1.258 feet
C_l	Rolling moment coefficient, rolling moment/ qSb
C_{l_α}	Slope of rolling moment coefficient curve vs α , rad^{-1}
C_{l_β}	Slope of rolling moment coefficient curve vs β , rad^{-1}
$C_{l_p} + C_{l_{\dot{\beta}}} \sin \alpha$	Total damping in roll derivative, rad^{-1}
$C_{l_q} + C_{l_{\dot{\alpha}}}$	Cross-coupling derivative of rolling moment due to pitch-oscillation, rad^{-1}
$C_{l_r} - C_{l_{\dot{\beta}}} \cos \alpha$	Cross derivative of rolling moment due to yaw-oscillation, rad^{-1}
C_m	Pitching moment coefficient, pitching moment/ $q S \bar{c}$
C_{m_α}	Slope of the pitching moment coefficient curve vs α , rad^{-1}
C_{m_β}	Slope of the pitching moment coefficient curve vs β , rad^{-1}
$C_{m_q} + C_{m_{\dot{\alpha}}}$	Total damping in pitch derivative, rad^{-1}
$C_{m_r} - C_{m_{\dot{\beta}}} \cos \alpha$	Cross-coupling derivative of pitching moment due to yaw-oscillation, rad^{-1}
C_N	Normal force coefficient, normal force/ $q S$
C_{N_α}	Slope of normal force coefficient vs α , rad^{-1}
C_{N_β}	Slope of normal force coefficient vs β , rad^{-1}
$C_{N_q} + C_{N_{\dot{\alpha}}}$	Damping in normal force derivative, rad^{-1}
C_n	Yawing moment coefficient, yawing moment/ qSb
C_{n_α}	Slope of yawing moment coefficient vs α , rad^{-1}
C_{n_β}	Slope of yawing moment coefficient vs β , rad^{-1}

$C_{n\dot{p}} + C_{n\dot{\beta}} \sin \alpha$	Cross derivative of yawing moment due to roll oscillation, rad^{-1}
$C_{nq} + C_{n\dot{\alpha}}$	Cross-coupling derivative of yawing moment due to pitch oscillation, rad^{-1}
$C_{nr} - C_{n\dot{\beta}} \cos \alpha$	Total damping in yaw derivative, rad^{-1}
C_Y	Side force coefficient, side force/qS
$C_{Y\alpha}$	Slope of C_Y vs α , rad^{-1}
$C_{Y\beta}$	Slope of C_Y vs β , rad^{-1}
$C_{Yr} - C_{Y\dot{\beta}} \cos \alpha$	Damping in side force derivative, rad^{-1}
E	Voltage excitation amplitude, volts
f	Frequency, hz
f_n	Natural frequency, hz
F_N	Static normal force on model, lb
FS	Fuselage station measured from nose, in.
F_Y	Static side force on model, lb
I_{xx}, I_{yy}, I_{zz}	Mass moments of inertia about the x, y, and z axes, respectively, slug-ft ² or lb _f -in.-sec ²
I_{y_0}	Inertia of calibration body, 1.857 lb _f -ft-sec ²
M	Mach number
m	Total mass of moveable calibration weights, 1.6628 slugs
M_r	Static rolling moment, ft-lb
M_{rI}	In-phase rolling moment, ft-lb
M_{rQ}	Out-of-phase rolling moment, ft-lb
M_m	Static pitching moment on model, ft-lb
M_{mI}	In-phase pitching moment, ft-lb
M_{mQ}	Out-of-phase pitching moment, ft-lb
M_n	Static yawing moment, ft-lb

M_{nI}	In-phase yawing moment, ft-lb
M_{nQ}	Out-of-phase yawing moment, ft-lb
$MS2$	Static sting moment, ft-lb
$MS2I$	In-phase sting moment, ft-lb
$MS2Q$	Out-of-phase sting moment, ft-lb
$M_{\theta f}$	Spring constant 6294.7 ft-lb/rad for P/Y balance, or 1468.0 ft-lb/rad for roll balance lb/rad
p	Free-stream static pressure, psfa
p	Rolling velocity, radians/sec
p_c	Test section plenum chamber pressure, psfa
P_t	Tunnel stilling chamber pressure, psfa
q	Free-stream dynamic pressure, psfa
q	Pitching velocity, radians/sec
r	Yawing velocity, radians/sec
Re/ft	Free-stream Reynolds number, ft^{-1}
RFP	Reduced frequency parameter $(\omega \cdot \bar{c})/2V$ for pitch phase, $(\omega \cdot b)/2V$ for yaw and roll phases, radians
S	Reference model wing area, 3.704 ft^2
S	Precision index, i.e. computed standard deviations of the measurements
TORI	In-phase forcing torque, ft-lb
TORQ	Quadrature forcing torque, ft-lb
T_t	Tunnel stilling chamber temperature, °F
t	Time, sec
t_{95}	The 95th percentile point for the two-tailed Student's "t" distribution, $t_{95} = 2.0$ if degrees of freedom exceed 30
U	Estimated uncertainty

V	Free-stream velocity, ft/sec
WL	Water line, in.
WT	Model weight, lb
x, y, z	Model coordinates, in.
α	Model angle of attack, deg
$\dot{\alpha}$	Time rate of change of α , radians/sec
β	Model sideslip angle, deg
$\dot{\beta}$	Time rate of change of β , radian/sec
ΔX	Distance of calibration weight from pivot center, ft
$\Delta\phi$	Phase shift, deg
ΔI_{yy}	Moment of inertia between can load cell and pivot axis of forced oscillation balance, slug-ft ²
δ_e	Horizontal stabilizer (stabilator) deflection, deg
δ_{LE}	Leading edge flap deflection, deg
ζ	Damping ratio
$\bar{\theta}$	Model oscillation amplitude, deg or rad
ω	Angular rate of oscillation, $\omega = 2\pi f$, rad/sec
ω_n	Natural rate of oscillation, $\omega_n = 2\pi f_n$, rad/sec
SUBSCRIPT	
n	Natural
Tare	Tare value, wind-off